

Manifold learning with sparse regularised optimal transport

Stephen Zhang^{*1}, Gilles Mordant^{*2}, Tetsuya Matsumoto³, and Geoffrey Schiebinger³

¹University of Melbourne

²Universität Göttingen

³University of British Columbia

July 20, 2023

Abstract

Manifold learning is a central task in modern statistics and data science. Many datasets (cells, documents, images, molecules) can be represented as point clouds embedded in a high dimensional ambient space, however the degrees of freedom intrinsic to the data are usually far fewer than the number of ambient dimensions. The task of detecting a latent manifold along which the data are embedded is a prerequisite for a wide family of downstream analyses. Real-world datasets are subject to noisy observations and sampling, so that distilling information about the underlying manifold is a major challenge. We propose a method for manifold learning that utilises a symmetric version of optimal transport with a quadratic regularisation that constructs a *sparse* and *adaptive* affinity matrix, that can be interpreted as a generalisation of the bistochastic kernel normalisation. We prove that the resulting kernel is consistent with a Laplace-type operator in the continuous limit, establish robustness to heteroskedastic noise and exhibit these results in simulations. We identify a highly efficient computational scheme for computing this optimal transport for discrete data and demonstrate that it outperforms competing methods in a set of examples.

1 Introduction

Real-world datasets are increasingly high-dimensional with imaging and biological measurements frequently being made in tens of thousands of dimensions. Typically however the degrees of freedom intrinsic to the underlying process being observed are far fewer than the number of observed dimensions, and the data points concentrate on a latent lower dimensional subset of the ambient high-dimensional space. Noise on the other hand is abundant, both in terms of measurement error as well as naturally arising variability, and can be assumed corrupt measured data points in the ambient space. To provide a concrete example, each data point in the MNIST dataset has an intrinsic dimensionality of around 15 (Hein and Audibert, 2005), even though the pictures are $28 \times 28 = 784$ pixels large. The first step towards tackling the challenge of extracting useful signal from noisy high dimensional datasets is to identify this latent lower dimensional structure. To do so, analysis workflows almost always rely on affinity matrices or neighbourhood graphs that capture the local geometry, as we will develop upon in Section 1.1.

In recent years, the utility of optimal transport and related ideas to applications in statistics and data science has been acknowledged by many groups for a plethora of purposes: biology (Schiebinger et al., 2019; Zhang et al., 2021; Lavenant et al., 2021), statistics (Hallin, Mordant, and Segers, 2021; Hallin et al., 2021; Nies, Staudt, and Munk, 2021; Zhang, 2021; Hundrieser, Staudt, and Munk, 2022; Mordant and Segers, 2022; Hundrieser et al., 2023), machine learning (Cuturi, 2013; Gulrajani et al., 2017; Feydy et al., 2019), and economics (Carlier, Chernozhukov, and Galichon, 2016; Torous, Gunsilius, and Rigollet, 2021; Hallin and Mordant, 2022), to name a few. This list is by no means exhaustive and we encourage the interested reader to consult the references therein.

We show that manifold learning is one further domain where we draw on inspiration from optimal transport. We provide the required background on optimal transport for this particular setting in Section 1.2 before summarising the main contributions of this paper in Section 1.3. Section 2 then contains our theoretical results and investigations, Section 3 presents further use cases and simulations. We conclude by stating a few open questions for further study in Section 4. Additional elements and proofs are provided in the appendices.

*Both authors contributed equally.

1.1 Manifold learning: graphs, affinity matrices, and operators

The setting we consider in this paper is a d -dimensional, compact and smooth Riemannian manifold (\mathcal{M}, g) isometrically embedded in \mathbb{R}^p via the embedding $\iota : \mathcal{M} \hookrightarrow \mathbb{R}^p$, with the ambient dimension p being much larger than the intrinsic dimension d . In what follows, we denote by ι_* , the differential of this embedding. Our observations are a set of points sampled from the manifold, $\mathcal{X} = \{x_i\}_{i=1}^N \subset \mathbb{R}^p$ where each x_i is produced by embedding a point $y_i \in \mathcal{M}$ into \mathbb{R}^p , possibly with noise. These can be random or deterministic in nature. In the random case, one may consider the y_i to be sampled according to some density p supported on \mathcal{M} . Then, let

$$C_{ij} = C(x_i, x_j) = \frac{1}{2} \|x_i - x_j\|_2^2$$

be the matrix of pairwise distances measured in the ambient Euclidean space \mathbb{R}^p . Let $\mu = N^{-1} \sum_i \delta_{x_i}$ be the empirical measure constructed from the observed point set.

1.1.1 Affinity matrices

Starting from pairwise distances in the ambient Euclidean space, the characteristic workflow for a majority of manifold learning approaches (Coifman et al., 2005; Saul and Roweis, 2000; Tenenbaum, Silva, and Langford, 2000; Zhang and Zha, 2004) is to construct from C_{ij} an affinity matrix $W_{ij} \geq 0$ which can be thought of as capturing local information in the adjacency matrix of a weighted graph. Affinity matrices are sometimes referred to as *kernel* matrices, although in general they may fail to be positive semidefinite and thus are not strictly kernels. Pairs of points in close proximity (as measured in the ambient space) are assigned a high affinity, and pairs that are far away are assigned a low (or zero) affinity. One of the most common constructions is to build W such that each point x_i is connected by an edge to its k nearest neighbours. The goal of W therefore is to encode only local relationships: since by assumption \mathcal{M} is smooth, the ambient Euclidean metric locally agrees with the Riemannian metric. Following this reasoning, the weighted graph generated by W is a reasonably faithful representation of the latent manifold \mathcal{M} .

1.1.2 Laplacian operators

A key characterisation of the matrix W is its that it defines a (discrete) linear operator acting on vectors supported on \mathcal{X} , the set of points sampled from the manifold \mathcal{M} . Under the interpretation of W as a weighted graph, there is naturally the notion of a Laplacian matrix:

$$L = D - W, \quad D = \text{diag}(W\mathbf{1}).$$

The eigenvectors of L may then be used as basis functions to represent observed data in a lower dimensional space that is adapted to the geometry of the latent manifold, as in Coifman and Lafon, 2006 for instance. More generally, we consider the construction of a family of discrete linear operators on square-integrable functions supported on \mathcal{X} of the type

$$\Delta^D : L^2(\mathcal{X}) \rightarrow L^2(\mathcal{X}), \quad (\Delta^D g)(x_i) := \sum_{j=1}^N W_{ij} (g(x_i) - g(x_j)). \quad (1)$$

Treated as a discrete analogue to the Laplace—Beltrami operator (von Luxburg, Belkin, and Bousquet, 2008), the graph Laplacian enjoys a wealth of interpretations and uses. Indeed, the corresponding Dirichlet form is fundamental in the computation of eigenfunctions via the Courant—Fisher—Weyl min-max principle (Bhatia, 2013, Section III.1) leading to the vast toolbox of spectral methods for clustering and embedding (von Luxburg, 2007; Belkin and Niyogi, 2003). As another example, the discrete Laplacian is connected to random walks and diffusion processes, yielding a discrete heat kernel from which geodesic distances can be estimated by utilising the connection to heat propagation (Crane, Weischedel, and Wardetzky, 2013), a fact that has been utilised in applications to mass transport on manifolds (Solomon et al., 2015). Laplace-based methods are foundational to applications in computer geometry (Lévy, 2006; Reuter, Wolter, and Peinecke, 2006), and more generally in machine learning applications where Laplacian regularisations are used to adapt models to manifold or graph structures in datasets Belkin, Niyogi, and Sindhwani, 2006; Cai et al., 2008.

1.2 From bistochastic normalizations to sparse regularised optimal transport

1.2.1 Normalisation of the Laplacian matrix

In practice, the sampled data $\{x_i\}_{i=1}^N$ may be subject to variable sampling density and noise in the high-dimensional ambient space. The Laplacian matrix can be normalised in various fashions in order to account for the effects of variable sampling density as well as to have desirable properties for subsequent analyses. Laplacian eigenmaps (Belkin and Niyogi, 2003) and diffusion embeddings (Coifman et al., 2005) are two closely related examples of classical nonlinear manifold learning approaches that utilise the spectral decomposition of a normalised Laplacian. Two of the most common normalisation choices are the symmetric normalisation, $L^{(s)} = I - D^{-1/2}WD^{-1/2}$, which preserves the symmetric positive semidefinite property, and the random-walk or Markov normalisation, $L^{(rw)} = I - D^{-1}W$, which affords a probabilistic interpretation as the generator of a diffusion process. A particularly interesting approach is that of Coifman and Lafon (2006), where a family of anisotropic diffusions are constructed by normalising a kernel matrix by a positive power of its row sums. The normalised kernels are shown to have different interpretations for varying choices of α , and for an appropriate value of α the authors demonstrate that the effect of sampling density is decoupled from geometry.

1.2.2 Bistochastic normalisations are information projections

Significant interest has been devoted to *bistochastic* normalizations of affinity matrices, which enjoy both the symmetry property as well as the probabilistic interpretation related to random walks (Marshall and Coifman, 2019; Landa, Coifman, and Kluger, 2021). This is particularly favourable for the manifold learning setting, as the Laplace-Beltrami operator itself is both self-adjoint and generates the heat kernel on appropriate manifolds (Grigoryan, 2009, Chapters 3 & 7). Recently, Landa, Coifman, and Kluger (2021) investigated the bistochastic scaling of the positive semi-definite Gaussian kernel $W_\varepsilon = \exp(-C/\varepsilon)$ of the form

$$W_\varepsilon^{(d)} = \text{diag}(d)W_\varepsilon \text{diag}(d),$$

where $d > 0$ is a vector of multiplicative scaling factors applied to both the rows and columns of W . As discussed in their article, the normalised kernel $W_\varepsilon^{(d)}$ can be characterised as an information projection, i.e. with respect to the Kullback-Leibler (KL) divergence. That is:

$$W_\varepsilon^{(d)}(C) := \underset{A \in \mathcal{K}}{\text{argmin}} \text{KL}(A|W_\varepsilon) \quad (2)$$

$$= \underset{A \in \mathcal{K}}{\text{argmin}} \frac{1}{\varepsilon} \langle A, C \rangle + \text{KL}(A|\mathbf{1}\mathbf{1}^\top), \quad (3)$$

where $\text{KL}(A|W) = \sum_{ij} A_{ij} \log(A_{ij}/W_{ij})$ and \mathcal{K} denotes the set of *hollow*, symmetric, bistochastic kernel matrices, i.e. those with all zeros on the diagonal:

$$\mathcal{K} = \{A \in \mathbb{R}_{\geq 0}^{N \times N} : A\mathbf{1} = \mathbf{1}, A = A^\top, \text{diag}(A) = 0\}.$$

The requirement on the diagonal removes self connections, which was shown to be crucial for rendering the procedure robust to heteroskedastic noise in (Landa, Coifman, and Kluger, 2021). Here the projection is computed with respect to the KL-divergence, but in general a different divergence can be used. Another interpretation of the problem is as an symmetric *optimal transport* problem with entropic regularisation. This problem can be solved efficiently in practice using the celebrated Sinkhorn matrix scaling algorithm (Cuturi, 2013).

1.2.3 Projections in the Frobenius norm

One consequence of using an information projection is that the resulting kernel matrix is always strictly positive and so the graph is fully connected, which is at odds with the fact that manifolds are only locally homeomorphic to the Euclidean space. Zass and Shashua (2006) proposed to consider the projection of a given kernel matrix is sought with respect to the Frobenius norm, which induces sparsity in the projected matrix. This will be our starting point: substituting the Frobenius norm in place of the KL-divergence in (3), we arrive at a *hollow quadratically* regularised optimal transport problem

$$W_\varepsilon^{(f)}(C) := \underset{A \in \mathcal{K}}{\text{argmin}} \frac{1}{\varepsilon} \langle A, C \rangle + \|A\|_F^2 \quad (4)$$

$$= \underset{A \in \mathcal{K}}{\text{argmin}} \|A + \varepsilon^{-1}C\|_F^2. \quad (5)$$

Whenever clear from context, we will drop the argument C of $W_\varepsilon^{(f)}(C)$. It is apparent from (5) that this amounts to a bistochastic projection with respect to Frobenius norm of a negative distance matrix $-C/\varepsilon$. While this matrix itself is not positive semidefinite, since $C_{ij} = \|x_i\|^2/2 + \|x_j\|^2/2 - \langle x_i, x_j \rangle$ it is the sum of the linear kernel matrix and two rank-1 terms. It will be apparent in Section 2.2 that the latter two terms are immaterial. The problem of optimal transport with a quadratic regularisation was studied in detail by Lorenz, Manns, and Meyer (2021) and Essid and Solomon (2018), and for completeness we provide a discussion in Appendix A.1. Similarly to Lorenz, Manns, and Meyer (2021, Equation D), the primal problem (4) admits a counterpart of the following dual problem involving a Lagrange multiplier u ,

$$\max_u \langle u, \mathbf{1} \rangle - \frac{1}{4\varepsilon} \|[u\mathbf{1}^\top + \mathbf{1}u^\top - C]_+ \odot (\mathbf{1}\mathbf{1}^\top - I)\|_F^2, \quad (6)$$

where $[x]_+$ is the positive part of x applied elementwise and D a positive diagonal matrix, as follows from Lemma 4. This is a convex non-smooth problem: denoting by u^* the optimal solution of (6), the projection A can be recovered from the optimal potential vector u^* by

$$W_\varepsilon^{(f)}(C) = \frac{1}{\varepsilon} [u^*\mathbf{1}^\top + \mathbf{1}u^{*\top} - C]_+ \odot (\mathbf{1}\mathbf{1}^\top - I). \quad (7)$$

From this characterisation of the projection solution, it becomes apparent that some off-diagonal entries may be identically zero —precisely, whenever $u_i^* + u_j^* \leq C_{ij}$.

The sparsity of the affinity matrix $W_\varepsilon^{(f)}$ leads to practical benefits for downstream tasks such as finding eigenvalue-eigenvector pairs, which partly makes up for the fact that the solution of the quadratically regularised problem (6) is slightly more expensive than the entropically regularised one. Additionally, as pointed out by Lorenz, Manns, and Meyer, 2021, the algorithm for computing the projection is stable with respect to the parameter ε . This is in contrast to the entropic case which is (in)famous for its numerical stability issues (Schmitzer, 2019).

1.2.4 A spectral motivation for the Frobenius norm

The bistochastic projection of an affinity matrix W with respect to the Frobenius norm can be understood as finding the best bistochastic matrix A in terms of the Davis-Kahan spectral upper bound. Considering the k leading eigenvalues of A and W respectively (and their eigenvectors), the Davis-Kahan theorem (Yu, Wang, and Samworth, 2015, Theorem 2) states that

$$\|\sin \Theta(V_k(A), V_k(W))\|_F \leq \frac{2\|W - A\|_F}{\lambda_k(W) - \lambda_{k+1}(W)}.$$

In the above, the left-hand side is the norm of the matrix of (sines of) pairwise principal angles. This measures how close the leading k eigenspaces of A and W are. For $1 \leq k \leq N$, $\lambda_k(W)$ is the k th eigenvalue (in descending order) of an affinity matrix W , and $V_k(W)$ is the matrix with orthonormal columns formed from the leading k eigenvectors of W . In our context W is a fixed noisy affinity matrix determined by our data, and so only the numerator is of relevance. Among all bistochastic affinity matrices we consider, the one that is most faithful to the spectrum of the observed affinities W as measured by the Davis-Kahan upper bound is therefore the one that is closest in Frobenius norm. This insight agrees with our empirical observations that the Frobenius projection has better spectral properties compared to the information projection. Note however that, as we shall see in the robustness section, the method is invariant with respect to some types of noise, implying that one indeed finds a faithful representation of the unknown truth.

1.2.5 Generalised bistochastic information projections

In the above, we have discussed two frameworks for finding bistochastic projections of kernel matrices. One is in terms of an information projection of a Gaussian kernel matrix, and the other is a projection of minus the matrix of pairwise distances in the Frobenius norm. We now show that both manifest as two special cases of a generalised information projection of the same linear kernel matrix. While we defer details to Appendix A.1, note that for $q \in [0, 1)$ a generalised family of exponential and logarithm functions can be defined (Bao and Sakaue, 2022) by

$$\exp_q(x) = [1 + (1 - q)x]_+^{1/(1-q)}, \quad \log_q(x) = (1 - q)^{-1}(x^{1-q} - 1).$$

We remark that as $q \rightarrow 1$ we recover the conventional exponential and logarithm. This leads to an analogue Φ_q of the relative entropy functional being defined on matrices, and its generator ϕ_q , given by

$$\Phi_q(A|B) = \frac{1}{2-q} \sum_{i,j} \left[A_{ij} \log_q A_{ij} - A_{ij} \log_q B_{ij} - A_{ij} B_{ij}^{1-q} + B_{ij}^{2-q} \right],$$

$$\phi_q(x) = \frac{1}{2-q} (x \log_q x - x),$$

Indeed when $q = 0$ this corresponds to the squared Frobenius norm $\frac{1}{2} \|A - B\|_F^2$, and when $q \rightarrow 1$ one recovers the KL-divergence. We find that a family of bistochastic projections for $q \in [0, 1)$ can be written

$$\operatorname{argmin}_{A \in \mathcal{K}} \varepsilon \Phi_q^* \left(\frac{-C}{\varepsilon}, \nabla \phi_q(A) \right),$$

where Φ^* denotes the Legendre dual of Φ . When $q = 0$ we recover the Frobenius norm projection of $-C/\varepsilon$, and as $q \rightarrow 1$ we recover the information projection of $\exp(-C/\varepsilon)$.

Curiously, the Gaussian kernel arises naturally from the linear kernel in this framework since $\phi_q(x) \rightarrow x \log x - x$. This suggests that the *linear* kernel is the natural one when using a Frobenius projection, and using alternative kernels amount to mapping first to a reproducing kernel Hilbert space (RKHS). Much in the same way, the Gaussian kernel is the natural one for information projection. We emphasise that this insight is in contrast to previous works (Zass and Shashua, 2006; Ding et al., 2022; Landa, Coifman, and Kluger, 2021; Landa and Cheng, 2022; Marshall and Coifman, 2019) which are less discriminate in the choice of kernel matrix; for instance considering projections of an arbitrary kernel matrix, or the Frobenius projection of a Gaussian kernel matrix. This is relevant to the setting of manifold learning: in contrast to clustering applications (Zass and Shashua, 2006) where input mappings to an RKHS are potentially of no consequence to the clustering results, for manifold learning one should use the linear (Euclidean) kernel since it locally coincides with the metric of the embedded manifold.

1.2.6 Geometric view on the optimisation problem

In the field of manifold learning, the local covariance matrix is paramount —see Malik et al. (2019) and the references therein. Indeed, it captures the geometry of the manifold at a point. Its truncated inverse can then be used in a Mahalanobis distance to approximate the geodesic distance on the manifold¹. The empirical local covariance matrix at x_j can be defined, for a *neighbourhood selector* matrix A as $C_A(x_i) := (X - x_i)^\top A^\top A (X - x_i)$.

For example, in Malik et al. (2019), they consider a matrix containing 0 zeros at the places corresponding to elements far from x_j , while having value $(\mathbf{1}^\top A \mathbf{1})^{-1/2}$ otherwise. The problem (4), can be rewritten using this notion of a neighbourhood selector as

$$\inf_{A \in \mathcal{K}} \sum_{i=1}^n \sum_{j=1}^n \operatorname{tr} (\|x_i - x_j\|^2 A_{i,j}) + \varepsilon \sum_{i=1}^n \sum_{j=1}^n A_{i,j}^2 = \inf_{A \in \mathcal{K}} \sum_{i=1}^n \operatorname{tr} (C_A(x_i)) + \varepsilon \sum_{i=1}^n \sum_{j=1}^n A_{i,j}^2$$

so that the problem can be interpreted as find a matrix A that balances the mean empirical local variances² while controlling for locality. The fact that the resulting matrix is sparse is then a desirable/necessary feature. Indeed, a Riemannian manifold is only locally homeomorphic to the Euclidean space and dense matrices A will likely give rise to corrupted/biased local correlation matrices. This explains why the density of points must therefore be taken into account as well as the local geometry and why the proposed method is appealing. Importantly, the relationship above is true only if one takes the squared Euclidean distance as a cost function. This explains why it is not indicated to take any arbitrary affinity matrix to carry out manifold learning; for clustering, the situation is different.

1.3 Contributions

In this work, we:

¹More precisely, denoting by $C_\varepsilon(x)$ the ε local covariance matrix centred at x and by T_α the maps sending a matrix $n \times n$ A onto $U_A(\Lambda(A)^{-1} \odot \operatorname{diag}(1_\alpha, 0_{n-\alpha})) U_A^\top$ ($\alpha \leq n$), the geodesic distance can be approximated by

$$(x - y)^\top (T(C_\varepsilon(x)) + T(C_\varepsilon(y))(x - y))/2,$$

where α and ε have to be chosen properly.

²Recall that the sum of eigenvalues of a covariance matrix is the variance.

- suggest a manifold learning procedure based on a new variation of quadratically regularised optimal transport that generalises the problem of bistochastic kernel scaling;
- investigate its theoretical properties: we show its robustness to non-uniform noise, study the limit of discrete operators, and exhibit a similarity with the solution of the porous medium equation;
- exhibit its performance in simulated examples as well as in real-data applications.

We briefly describe the above in the following subsections, while the corresponding results are developed in Sections 2 and 3.

1.3.1 Optimal transport-based manifold learning

The main idea of the paper is to use the bistochastic and sparse affinity matrix $W_\varepsilon^{(f)}$ obtained as the solution to the quadratically regularised optimal transport problem (8) for constructing a weighted neighbourhood graph in statistical settings. In particular, we advocate for its use in manifold learning. With this aim in mind, the spectral decomposition of $W_\varepsilon^{(f)}$ is of particular interest. In practice, the problem (4) can efficiently be solved numerically using a variety of methods: a variant of the Newton-type algorithm proposed by Lorenz, Manns, and Meyer (2021) can be relied on (see Algorithm 1). It converges in relatively few iterations in practice and the key computation for each step involves iterative solution of a sparse linear system. Furthermore, the sparsity of the solution can be leveraged for further speedups (see Algorithm 2). As shall be seen in Section 3, the proposed method performs well in a variety of settings. We believe this to be the result of the *local-to-global* character of the construction. Indeed, as the resulting plan is sparse, with each node only connected to its neighbouring points. Yet, as the optimisation problem involves the entire distance matrix, the optimal dual potential incorporates more than just local information. In this sense, unlike approximation methods such as k - or ϵ -nearest neighbours which ensure local properties only, we do not sacrifice global information in favour of local information.

1.3.2 Sketch of the theoretical results

We will first set up a few more notations. Let μ be the (empirical or continuous) measure of points from the embedded manifold, and denote by $C(x, y) = \frac{1}{2}\|x - y\|_2^2$ the squared Euclidean distance function in \mathbb{R}^p . To be consistent in both discrete and continuous cases, we write

$$\pi^* = \operatorname{argmin}_{\pi \in \mathcal{K}} \left\| \pi - \frac{1}{\varepsilon}(-C) \right\|_{\mu \otimes \mu}^2 = \operatorname{argmin}_{\pi \in \mathcal{K}} \langle C, \pi \rangle_F + \frac{\varepsilon}{2} \|\pi\|_{\mu \otimes \mu}^2 \quad (8)$$

where $\mathcal{K} = \{\pi : \pi(A \times \mathcal{X}) = \pi(\mathcal{X} \times A) = \mu(A), \frac{d\pi}{d\mu \otimes d\mu}(x, x) = 0 \forall x\}$ denotes the set of symmetric positive measures that have marginals (μ, μ) . We remark that the hollowess condition from the discrete setting vanishes in the continuous setting, since then a pointwise requirement on the density of π along its *diagonal* has no effect. We write $\|\pi\|_{\mu \otimes \mu}^2 = \langle \frac{\pi}{\mu \otimes \mu}, \pi \rangle$ to mean the squared norm of $\frac{d\pi}{d\mu \otimes d\mu}$ in the space $L^2(\mu \otimes \mu)$.

The dual problem and the primal-dual relationship at optimality are then

$$\begin{aligned} \max_u \langle u, \mu \rangle - \frac{1}{4\varepsilon} \|[u \oplus u - C]_+(\mu \otimes \mu)\|_{\mu \otimes \mu}^2, \\ \pi^* = \frac{[u^* \oplus u^* - C]_+}{\varepsilon}(\mu \otimes \mu). \end{aligned} \quad (9)$$

Therefore, the optimal potential u^* must satisfy

$$\frac{1}{\varepsilon} \int [u^*(x) + u^*(y) - C(x, y)]_+ d\mu(y) = 1, \quad \forall x \in \mathcal{X} \quad (10)$$

Notice that for the discrete setting one can straightforwardly recover the equations (6), (7) from their continuous equivalents (9), (10) by setting $\mu = \mathbf{1}$, i.e. the counting measure.

The main theoretical contributions are robustness to heteroskedastic noise, proving the convergence of a first order approximation of the affinity kernel and exhibiting a link with the porous medium equation. Let us start with robustness to heteroskedastic noise. Following Landa, Coifman, and Kluger (2021, Theorem 3) and recalling the setup of Section 1.1, we consider a fixed set of points $\{y_i\}_{i=1}^N$ on the d -dimensional manifold \mathcal{M} that is then embedded in the p -dimensional Euclidean space to yield $\{x_i\}_{i=1}^N$.

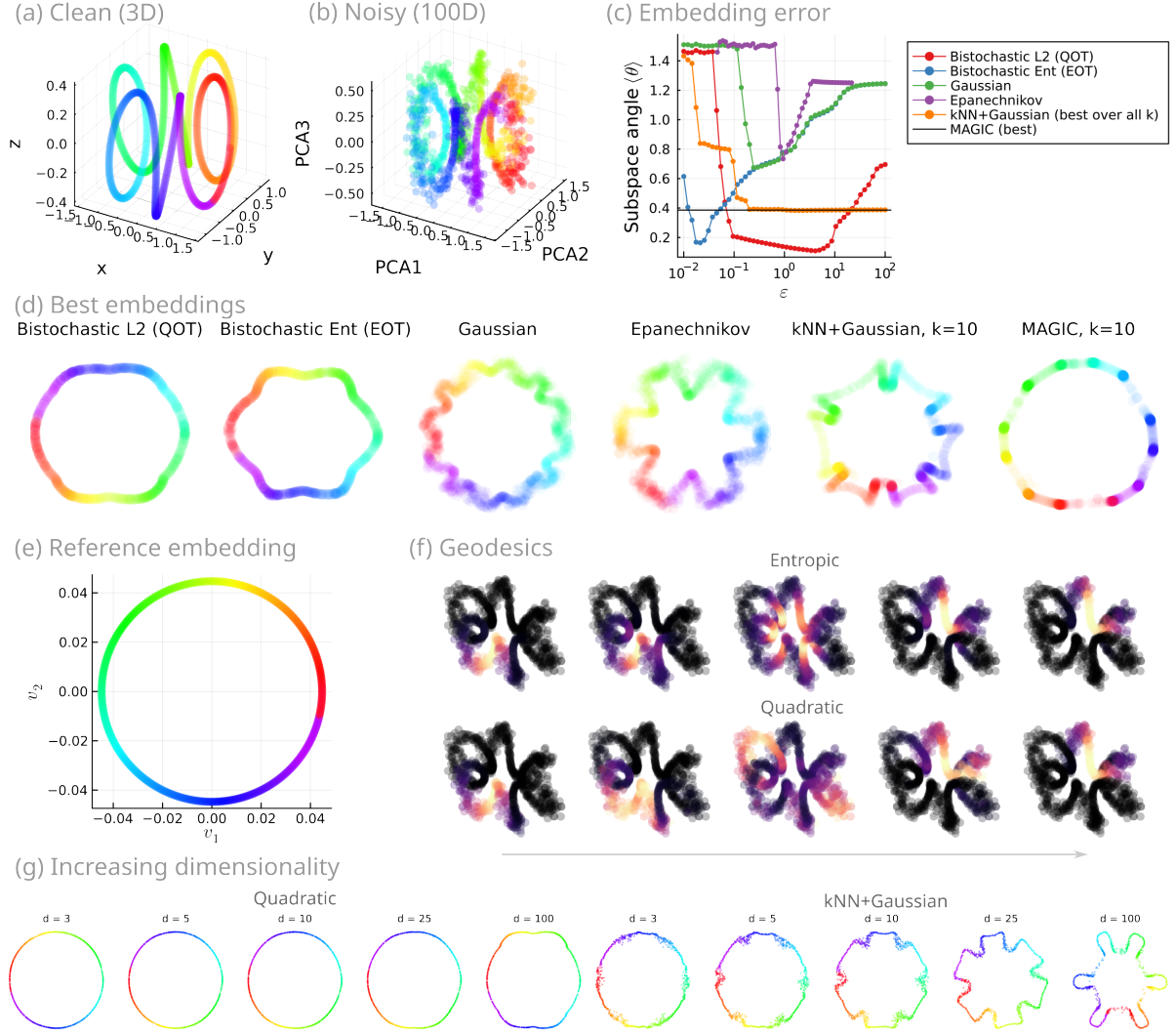


Figure 1: **Spiral with non-uniform noise.** (a) Clean points ($N = 1000$) sampled from spiral in 3 dimensions. (b) Points embedded in 100 dimensions subjected to non-uniform noise in high dimension. (c) Spectral embedding error (measured in terms of subspace angle) for the spectral embeddings obtained using various choices of kernel construction and bandwidth parameter (ϵ) choices. (d) Best embeddings found for each kernel construction. (e) Reference embedding produced from clean points in 3 dimensions. (f) Displacement interpolations computed as Sinkhorn barycenters using reference kernels from the entropic and quadratic kernel constructions respectively. (g) For fixed parameters, the spectral embedding obtained using the quadratic bistoochastic projection (Quadratic) and k -NN with Gaussian weights (kNN+Gaussian) with the top d PCA coordinates as d ranges from 3 (the dimensionality of the clean data) to 100 (the dimensionality of the noisy data).

We consider the setting where the ambient dimension increases $p \rightarrow \infty$. We next let these embedded points be contaminated by heteroskedastic additive noise, i.e.,

$$\tilde{x}_i = x_i + \eta_i, \quad (11)$$

with $\mathbb{E}[\eta_i] = 0$ and $\mathbb{E}[\eta_i \eta_i^\top] = \Sigma_i$.

Assume further that although the set of points prior to embedding is fixed, there exists some constant $\kappa > 0$ such that $\|x_i\| \leq \kappa, i = 1, \dots, n$, and that $\|\Sigma_i\|_2 \leq \kappa_\eta p^{-1}$, which means that the noise does not concentrate too much in a particular direction. For some models, normalisation of the data by \sqrt{p} also ensure the condition that the latter condition holds (Landa, Coifman, and Kluger, 2021, Remark 2). Then for $i \neq j$,

$$\|\tilde{x}_i - \tilde{x}_j\|^2 \xrightarrow{P} \mathbb{E}\|\eta_i\|^2 + \|x_i - x_j\|^2 + \mathbb{E}\|\eta_j\|^2, \quad \text{as } p \rightarrow \infty.$$

This type of noise contamination is also well cancelled by the quadratically regularised optimal transport

plan. Indeed, if u^* is the optimal dual transport potential for the uncontaminated setting,

$$\tilde{u}_i^* := u_i^* + \mathbb{E}\|\eta_i\|^2$$

is an approximate optimal dual potential for the cost matrix $C_{ij} = \|\tilde{x}_i - \tilde{x}_j\|^2$ for p large. This intuition can also be quantified: this is the statement of next proposition, whose proof is given in Appendix A.3.

Proposition 1. *Consider the heteroskedastic noise model introduced in (11). Denote by \tilde{C} the squared Euclidean cost matrix based on the corrupted points \tilde{x}_i . Then,*

$$\|W_\varepsilon^{(f)}(C) - W_\varepsilon^{(f)}(\tilde{C})\| \leq \mathcal{O}_p(p^{-1/2}),$$

where \mathcal{O}_p refers to stochastic boundedness.

The main theoretical results of the paper, Theorem 1, pertains to the limiting distribution of the discrete Laplace operator based on the optimal transport plan and can be understood as follows. We refer to Section 2.3 for the full picture.

Theorem (Sketch of Theorem 1). *Consider a random sample $\{X_i\}_{i=0}^N$ independently and uniformly distributed on a smooth manifold embedded in \mathbb{R}^p and the first-order approximation $\bar{W}^{(f)}$ of $W_\varepsilon^{(f)}(C)$, combining Lemma 1 and the representation (7). Then, there exists a Laplace-type operator Δ^∞ and, for any fixed function $g \in C^2$, it holds that*

$$2K_{\varepsilon,N}^{-1} \sum_{j=0}^N \bar{W}_{0,j}^{(f)}(g(X_0) - g(X_j)) \xrightarrow{L^2} \Delta^\infty g,$$

where $K_{\varepsilon,N}$ is a well-chosen sequence depending on ε , N and choosing ε as an appropriate function of N .

Remark 1 (Convergence rates). It is important to note that, as the proof relies on quantification of the bias and the variance, convergence rates are implicitly given by the proof.

Our final observation is that plugging the first-order optimal dual potentials from Lemma 1 in the representation (7) gives a kernel which behaves like the Barenblatt–Prattle solution of the porous medium equation, see Section 2.5 for further details.

2 Theoretical statements

Let us now describe a bit more the manifold setting that we consider for random samples. Let X be a p -dimensional random variable whose range is supported on \mathcal{M} . Let us further assume for simplicity that X has a uniform distribution on the manifold, i.e., the density $dP(x) = \text{vol}^{-1}(\mathcal{M})dx, \forall x \in \iota(\mathcal{M})$. Whenever we write \mathbb{E} or Var , unless otherwise denoted we mean to be with respect to P . Let us denote by $s(x)$, the scalar curvature of the manifold at x and by \mathbb{I}_x the second fundamental form of the isometric embedding ι at x . In the sequel, ∇ will denote the covariant derivative while Δ will be the Laplace-Beltrami operator. Further, set

$$\omega(x) = \frac{1}{|S^{d-1}|} \int_{S^{d-1}} \|\mathbb{I}_x(\theta, \theta)\|^2 d\theta,$$

as well as

$$\mathfrak{N}(x) = \frac{1}{|S^{d-1}|} \int_{S^{d-1}} \mathbb{I}_x(\theta, \theta) d\theta,$$

where S^{d-1} denotes the $(d-1)$ -dimensional unit sphere in $T_x\mathcal{M}$.

For the sake of simplicity, let us make the following assumptions.

Assumption 1. *The manifold \mathcal{M} is correctly shifted and rotated so that $\iota_*T_{x_0}\mathcal{M}$ is spanned by e_1, \dots, e_d .*

Assumption 2. *The manifold is properly rotated and translated so that e_{d+1}, \dots, e_p diagonalise the second fundamental form \mathbb{I}_{x_0} .*

These two conditions are not particularly important, they just help simplify both notation and result statements. Under these assumptions, we use the notation $\llbracket v_1, v_2 \rrbracket$ for the vector v whose d first components are the vector v_1 and its $p - d$ last components are the vector v_2 . The $p \times r$ matrix $\tilde{J}_{p,r}$ is then defined as

$$\tilde{J}_{p,r} := \begin{pmatrix} 0_{p-r \times r} \\ I_{r \times r} \end{pmatrix}$$

In what follows, for some η sufficiently small, define the fattened manifold in the embedded space by \mathcal{N} , i.e. the set $\mathcal{N} := \{x \in \mathbb{R}^p : \inf_{y \in \mathcal{M}} \|x - \iota(y)\| \leq \eta\}$. We recall that the Laplace operator for a function g on a certain embedded smooth manifold $\iota(\mathcal{M})$ is defined for $p \in \iota(\mathcal{M})$ as

$$\Delta g(p) := (\Delta_{\mathbb{R}^p} g_{\text{ext}})(p)$$

with $\Delta_{\mathbb{R}^p}$ the usual Laplace operator in the Euclidean space, $g_{\text{ext}}(x) := g(\pi_{\mathcal{M}}(x))$, $x \in \mathcal{N}$, and $\pi_{\mathcal{M}}$ projects \mathcal{N} onto the manifold. For the entire paper, r *sufficiently small* must be understood as r being smaller than the injectivity radius of the manifold.

2.1 Nearly optimal potentials

We now turn to the study of the optimal rates for the potentials in the discrete case. Let us slightly change the setting and consider a sample of size $N + 1$ where one point, $x_0 \in \mathcal{M}$, is fixed and the remaining ones are an i.i.d. random sample on the manifold. Set $X_0 = \iota(x_0)$. We relabel the sampled points so that $\|X_0 - X_1\|^2 \leq \|X_0 - X_2\|^2 \leq \dots \leq \|X_0 - X_N\|^2$.

Remark 2 (No loss of generality in choosing X_0). In the results below, the same analysis can be carried out for each point X_i . One can thus view our (convenient) choice of working with one distinguished, deterministic point as a conditioning on an arbitrary X_i . Still, as the expectations of the quantities for X_0 fixed are constants with uniformly decaying terms, the reasoning would apply for each X_i using the tower property of conditional expectation.

Lemma 1. *The optimal potential must behave like*

$$u^* \sim K_{\varepsilon,N} := \left(\frac{\text{vol}(\mathcal{M})}{|S^{d-1}|} \frac{d(d+2)}{2} \right)^{\frac{2}{d+2}} \varepsilon^{\frac{2}{d+2}} N^{-\frac{4}{d+2}} = C_d \varepsilon^{\frac{2}{d+2}} N^{-\frac{4}{d+2}}.$$

These results provide a reasonable *ansatz*, still these are only approximations. We now assess the quality of this first order approximation of the solution by evaluating how the dual constraints are fulfilled when plugging-in the first-order approximation of the solution.

2.1.1 Validity of the derived finite sample rate

We will use the function

$$f(y) = C_d \varepsilon^{2/(d+2)} N^{-4/(d+2)} - \|\iota(x_0) - y\|^2 = K_{\varepsilon,N} - \|\iota(x_0) - y\|^2$$

and apply to the result of Lemma B.5 from Wu and Wu (2018) to evaluate the constraints arising from the dual formulation of the problem, recall (7) and (10). Doing so, one gets

$$\begin{aligned} & \mathbb{E} \left(\frac{N+1}{\varepsilon} \sum_{j=0}^N (K_{\varepsilon,N} - \|X_j - \iota(x_0)\|)^2_+ \right) \\ &= \frac{N+1}{\varepsilon} \left\{ K_{\varepsilon,N} + N \mathbb{E} \left[f(X) \mathbf{1} \left\{ \|\iota(x_0) - X\| \leq K_{\varepsilon,N}^{1/2} \right\} \right] \right\} \\ &= \frac{N+1}{\varepsilon} K_{\varepsilon,N} + \frac{N(N+1)}{\varepsilon} \frac{|S^{d-1}|}{d \text{vol}(\mathcal{M})} K_{\varepsilon,N}^{1+d/2} \\ &\quad + \frac{N(N+1)}{\varepsilon} \frac{|S^{d-1}|}{d(d+2) \text{vol}(\mathcal{M})} K_{\varepsilon,N}^{1+d/2} \left[-d + \frac{s(x_0) K_{\varepsilon,N}}{6} + \frac{d(d+2) \omega(x_0) K_{\varepsilon,N}}{24} \right] \\ &\quad + \frac{N(N+1)}{\varepsilon} \mathcal{O}(K_{\varepsilon,N}^{\frac{5+d}{2}}) \\ &= \frac{N+1}{\varepsilon} K_{\varepsilon,N} + \frac{N(N+1)}{\varepsilon} \frac{|S^{d-1}|}{\text{vol}(\mathcal{M})} K_{\varepsilon,N}^{1+d/2} \left(\frac{1}{d} - \frac{1}{d+2} \right) + \mathcal{O} \left(\frac{N(N+1)}{\varepsilon} K_{\varepsilon,N}^{2+d/2} \right) \end{aligned}$$

In the display above, terms have orders $\mathcal{O}(N\varepsilon^{-1}K_{\varepsilon,N}) = \mathcal{O}(\varepsilon^{-d/(d+2)}N^{(d-2)/(d+2)})$, $\mathcal{O}(N^2\varepsilon^{-1}K_{\varepsilon,N}^{2+d/2})$ and we remark that $\mathcal{O}(N^2\varepsilon^{-1}K_{\varepsilon,N}^{1+d/2}) = \mathcal{O}(1)$. This latter term is the leading order. Then, to fulfil the constraint, we need that

$$C_d^{\frac{2+d}{2}} \frac{|S^{d-1}|}{\text{vol}(\mathcal{M})} \left(\frac{1}{d} - \frac{1}{d+2} \right) = 1,$$

so we have verified by this different approach that

$$C_d = \left(\frac{\text{vol}(\mathcal{M})}{|S^{d-1}|} \frac{d(d+2)}{2} \right)^{\frac{2}{d+2}},$$

which matches with the expression above. One gets that the chosen rates for the potential gives the correct constraint in expectation at the first order.

One can rewrite the conditions that $\mathcal{O}(\varepsilon^{-d/(d+2)}N^{(d-2)/(d+2)}) = o(1)$ as $\varepsilon^{-d}N^{(d-2)} \rightarrow 0$ and the condition $\mathcal{O}(N^2\varepsilon^{-1}K_{\varepsilon,N}^{2+d/2}) = \mathcal{O}(K_{\varepsilon,N}) = o(1)$ as $\varepsilon^2N^{-4} \rightarrow 0$. Note that the latter condition was already somewhat required to apply Lemma B.5 from Wu and Wu (2018). Together, these results indicate that the asymptotic scaling on ε is $N^{1-2/d} \ll \varepsilon \ll N^2$ for the constraints to be asymptotically fulfilled in expectation. Note that in this analysis that ε need not go to zero asymptotically. Rather, the need is for ε to be asymptotically sufficiently small relative to N . See the remark below.

Remark 3. In the developments above, we considered a classical optimal transport without the hollow constraint. The only difference is the term $\mathcal{O}(N\varepsilon^{-1}K_{\varepsilon,N})$, which is asymptotically negligible.

Remark 4. In the developments above, the result holds uniformly in x_0 under quite mild assumptions as, for a closed³ and smooth manifold, the different kinds of curvatures appearing in the expansions are bounded, recall Remark 2.

Thanks to Remark 4, one can derive that all the constraints will asymptotically be fulfilled in expectation when replacing the sum of optimal potentials by $K_{\varepsilon,N}$.

Remark 5. There is a difference in scaling between the discrete and continuous settings in our analysis —to get empirical input distributions that are consistent with the continuous setting in the limit of large N , for samples X_1, \dots, X_N we take $\hat{\mu} = N^{-1} \sum_i \delta_{X_i}$ as the corresponding empirical distribution. Suppose π is an admissible coupling for such a discrete problem. Then π is concentrated on the support of $\hat{\mu} \otimes \hat{\mu}$ and admits a density, $(d\pi/d\hat{\mu} \otimes d\hat{\mu})(X_i, X_j) = N^2\pi_{ij}$. Then, note that the corresponding empirical entropy term would behave like

$$H(\pi|\hat{\mu} \otimes \hat{\mu}) = \int d\pi \log \left(\frac{d\pi}{d\hat{\mu} \otimes d\hat{\mu}} \right) = \sum_{ij} \pi_{ij} \log(N^2\pi_{ij})$$

Up to a constant, this is equal to the discrete entropy of π , i.e. $\sum_{ij} \pi_{ij} \log \pi_{ij}$. Thus, we expect no scaling behaviour between N and the entropic regulariser.

On the other hand, for the quadratic regulariser, one would have

$$\|\pi\|_{\hat{\mu} \otimes \hat{\mu}}^2 = \int \frac{d\pi}{d\hat{\mu} \otimes d\hat{\mu}} d\pi = \sum_{ij} \pi_{ij} \frac{\pi_{ij}}{N^{-2}} = N^2 \|\pi\|_F^2. \quad (12)$$

Thus, there is the presence of a factor N^2 . This can be understood in that N appears in the density of π w.r.t. empirical product measure, which is lost as an additive term in the case of a log, but remains in the quadratic case. Thus, noting that $\varepsilon N^{-2} \|\pi\|_{\hat{\mu} \otimes \hat{\mu}}^2 = \varepsilon \|\pi\|_F^2$, it is apparent that the requirement that the effective epsilon $\tilde{\varepsilon} = \varepsilon N^{-2} \rightarrow 0$ in the continuous setting corresponds to $\varepsilon \ll N^2$ in the discrete setting. This is in agreement with the scaling we derived earlier.

2.1.2 Replacing the optimum by a uniform approximation

Similarly to Lorenz, Manns, and Meyer (2021, Lemma 3.1), the Newton Hessian of the optimisation problem (9) is

$$\text{diag}(\sigma \mathbf{1}_{N+1}),$$

where

$$\sigma_{ij} = \begin{cases} 1 & \text{if } u_i + u_j - C_{ij} \geq 0, \\ 0 & \text{otherwise.} \end{cases}$$

³Recall that a manifold is closed if it is compact and without boundary.

Because of the constraints, the potential must be chosen such that $u_j > 0, \forall j \leq N + 1$. The function to optimise is thus strictly concave for the set of such potentials and thus admits a unique optimum.

The update step in the semismooth Newton algorithm used in and originally developed in Lorenz, Manns, and Meyer (2021) takes the form

$$G_{i,i}^{-1} \left(\sum_j (K_{\varepsilon,N} - c_{i,j})_+ - \frac{\varepsilon}{N+1} \right), \quad 1 \leq i \leq N,$$

when the regularisation parameter of the algorithm is set to zero. From (14) again, it holds that

$$\mathbb{E}G_{ii} = \mathcal{O}(NK_{\varepsilon,N}^{d/2}).$$

From this and the computations of Section 2.1.1, the expectation of the update step is of order

$$\begin{aligned} \frac{1}{NK_{\varepsilon,N}^{d/2}} \left(\mathcal{O}(K_{\varepsilon,N}) + \mathcal{O}(NK_{\varepsilon,N}^{2+d/2}) \right) &= \mathcal{O} \left(\varepsilon^{\frac{2-d}{d+2}} N^{\frac{-2(2-d)-(d+2)}{d+2}} \right) + \mathcal{O}(K_{\varepsilon,N}^2) \\ &= \mathcal{O} \left(\varepsilon^{\frac{2-d}{d+2}} N^{\frac{d-6}{d+2}} \right) + \mathcal{O}(K_{\varepsilon,N}^2) \\ &= \mathcal{O} \left(\varepsilon^{\frac{-d}{d+2}} N^{\frac{d-2}{d+2}} \varepsilon^{\frac{2}{d+2}} N^{\frac{-4}{d+2}} \right) + \mathcal{O}(K_{\varepsilon,N}^2), \end{aligned}$$

which goes to zero in view of the conditions on ε and N mentioned above.

2.2 Robustness and potential optimality of the method

A natural question arising is whether the approach we propose can *proven* to be optimal and if so, in what precise sense or context. Our first points address the robustness of the approach with respect to perturbations of the cost matrix, while the second provides a link with choices of kernels in statistical density estimation or regression problems.

2.2.1 Robustness

Robustness was already hinted at in the main contributions, see Section 1.3.2. We thus only provide additional elements and details here below.

Lemma 2. *Consider a cost matrix C and a perturbed version of it, $\tilde{C} = C + E$, where E is an error matrix resulting from measurement noise. Denote by $\pi_\varepsilon(C)$ the unique optimal transport plan corresponding to C obtained by solving (7). Then,*

$$\|W_\varepsilon^{(f)}(C) - W_\varepsilon^{(f)}(C + E)\|_F \leq \varepsilon^{-1} \|E\|_F.$$

Further, if E is a rank-one perturbation, i.e., $E = \eta \oplus \eta$, then,

$$W_\varepsilon^{(f)}(C) = W_\varepsilon^{(f)}(C + \eta \oplus \eta).$$

Proof. The first statement follows from the fact that the set of hollow bistochastic matrices is a closed and convex set. Computation of $W_\varepsilon^{(f)}(C)$ amounts to a projection of $-C/\varepsilon$ onto the set of hollow bistochastic matrices in Frobenius norm. The set of hollow bistochastic matrix can be rewritten as the intersection of two closed sets and is thus closed. It is a well known result that the metric projection onto a nonempty, closed convex set is contractive. For the second point, it is directly seen from the dual formulation (9), that if u^* is optimal for C , then $u^* + \eta$ is optimal for $C + \eta \oplus \eta$. \square

In contrast, conventional normalisation approaches such as the frequently used Markov normalisation (Van Dijk et al., 2018; Coifman and Lafon, 2006) and symmetric normalisation (Belkin and Niyogi, 2003) do not in general have the capacity to remove this type of rank-1 noise.

Remark 6 (Extension to RKHS). Looking at the form of (8) and noting that $C_{ij} = \|x_i\|^2/2 + \|x_j\|^2/2 - \langle x_i, x_j \rangle$, we see that the problem is equivalent to projecting the kernel matrix $K_{ij} = \langle x_i, x_j \rangle$ onto the set of bistochastic matrices under the Frobenius norm. Other kernel matrices can be used, depending on what underlying RKHS one aims to use. This choice can be made depending on the model one has in mind, choosing it so that most of the noise be well described by a rank-one perturbation of the affinity

matrix. For the Gaussian kernel for instance, it is directly seen that in the same noise model as in Section 1.3.2,

$$\begin{aligned} \exp\left(-\frac{1}{\varepsilon}\|\tilde{x}_i - \tilde{x}_j\|^2\right) &= \exp\left(-\frac{1}{\varepsilon}\|x_i - x_j\|^2\right) \exp\left(-\frac{1}{\varepsilon}\langle x_i - x_j, \eta_i - \eta_j \rangle\right) \exp\left(-\frac{1}{\varepsilon}\|\eta_i - \eta_j\|^2\right) \\ &= \exp\left(-\frac{1}{\varepsilon}\|x_i - x_j\|^2\right) (1 + \mathcal{O}_p(m^{-1/2})), \end{aligned}$$

provided that $\exp\left(-\frac{1}{\varepsilon}\|\eta_i - \eta_j\|^2\right) = 1 + \mathcal{O}_p(1)$. From the stability of the metric projection, one can also observe robustness to additive heteroskedastic noise using the Gaussian kernel for ε not too small.

2.2.2 QOT, nonparametric statistics and optimality

The form of the quadratically regularised optimal transport plan in (7) is very much alike an Epanechnikov kernel, which is very often used in nonparametric statistics with the form

$$u \mapsto \frac{\Gamma(2 + d/2)}{\pi^{\frac{d}{2}}} (1 - u^\top u) \mathbf{1}_{\{u^\top u \leq 1\}}.$$

The Epanechnikov kernel is often claimed to be the optimal non-negative kernel (in terms of asymptotic mean integrated square error) for the estimation of a twice differentiable density (although this statement has been debated (Tsybakov, 2008, Section 1.2.4)). Thus, the compactness of its support and the fact that the optimal dual potential is a function which is more adaptive to the data than a uniform bandwidth, may explain its favourable performance observed in the numerical examples we consider.

2.3 Convergence of approximate discrete operator

We can now state our main theorem. Note that we consider functions defined on the ambient space \mathbb{R}^p , as opposed to only on \mathcal{M} , since in manifold learning \mathcal{M} is unknown and the operator will thus be applied to function on \mathbb{R}^p .

Theorem 1. *Consider $g \in C^2(\mathbb{R}^p)$, $g : \mathbb{R}^p \rightarrow \mathbb{R}$. Denote by L_0 and Q_0 the gradient and Hessian of g at x_0 , respectively. To simplify notation, set $X_0 = x_0$. Take a sample $\{X_j\}_{j=1}^N$ from the uniform distribution on \mathcal{M} which is embedded in \mathbb{R}^p . Then, under Assumptions 1 and 2, defining*

$$\Delta^{OT} g(X_0) := \sum_{j=0}^N \bar{W}_{0,j}^{(f)} (g(X_0) - g(X_j)),$$

with $\bar{W}^{(f)}$ the approximate solution of the quadratically regularised OT problem $W_\varepsilon^{(f)}(C)$ as introduced in Section 1.3.2, it holds that

$$-2K_{\varepsilon,N}^{-1} \Delta^{OT} g(X_0) \xrightarrow{L^2} dL_0 \left[0, \frac{\tilde{J}_{p,p-d}^\top \mathfrak{N}(x_0)}{2} \right] + \frac{1}{2} \text{tr} \left[Q_0 \begin{pmatrix} I_{d \times d} & 0 \\ 0 & 0 \end{pmatrix} \right],$$

provided that $K_{\varepsilon,N} \rightarrow 0$ and $N/\varepsilon \rightarrow 0$ when $N \rightarrow \infty$.

2.4 Infinitesimal generator limit and spectral convergence

A relatively general analysis of the convergence of graph Laplacians was carried out by Ting, Huang, and Jordan (2010), wherein consistency results are established for a general class of constructions leveraging connections to diffusion processes. We remark that when \mathcal{M} is endowed with a uniform measure, a constant approximation of the potential is valid and so the operator resulting from quadratically regularised optimal transport falls under their framework (Ting, Huang, and Jordan, 2010, Theorem 3). The assumptions are compatible with the ones that we make here, namely that \mathcal{M} is a smooth, compact manifold, and the authors consider a general kernel of the form $K_N(x, y) = w_x^{(N)}(y) K_0\left(\frac{\|y-x\|}{h_N r_x^{(N)}(y)}\right)$.

In our setting where i.i.d. samples are drawn uniformly on \mathcal{M} , we invoke a constant potential approximation $u \sim \varepsilon^{\frac{2}{2+d}} N^{\frac{-4}{2+d}}$, we have (up to a multiplicative constant)

$$K_N(x, y) = \left[\varepsilon^{\frac{2}{2+d}} N^{\frac{-4}{2+d}} - \|y - x\|^2 \right]_+ = \left[1 - \left(\frac{\|y - x\|}{\varepsilon^{\frac{1}{2+d}} N^{\frac{-2}{2+d}}} \right)^2 \right]_+ = \varphi\left(\frac{\|y - x\|}{h^{(N)}}\right)$$

Where the choice of kernel is the Epanechnikov kernel $\varphi(r) = (1 - r^2)_+$. The condition under which their theorem holds is that $Nh^{m+2}/\log N \rightarrow \infty$. In our case, this simplifies to $\varepsilon/(N \log N) \rightarrow \infty$, and this is compatible with the range of scalings $N^{1-2/d} \ll \varepsilon \ll N^2$ from our previous analysis.

2.5 Similarity with the porous medium equation

Consider again the continuous problem (8). Following Lorenz, Manns, and Meyer (2021) we write $\pi \in L^2(\mathcal{M})$ to be the density of a candidate transport plan w.r.t. product measure on $\mathcal{M} \times \mathcal{M}$, i.e. $\int \pi(x, y) dx dy = 1$. Then, the optimal transport plan π^* in the quadratically regularised problem must satisfy

$$\frac{1}{\text{vol}(\mathcal{M})} \int_{\mathcal{M}} \pi^*(\iota(x_0), y) dy = \mathbb{E} [\pi^*(\iota(x_0), X)] = \frac{1}{\text{vol}(\mathcal{M})^2}.$$

Taking the relation $\pi^* = \varepsilon^{-1}[u^* \oplus u^* - C]_+$ where $u^* \in L^2(\mathcal{M})$ is the corresponding optimal dual potential, making the ansatz that $u^* \sim \varepsilon^\alpha$ and invoking (14) we have, for $\varepsilon \ll 1$,

$$\begin{aligned} \mathbb{E} \left[u^*(\iota(x_0)) + u^*(X) - \frac{1}{2} \|\iota(x_0) - X\|_2^2 \right]_+ &\sim \mathbb{E} \left[(\varepsilon^\alpha - \|X - \iota(x_0)\|^2) \mathbf{1}\{\|X - \iota(x_0)\| \leq \varepsilon^{\alpha/2}\} \right] \\ &\sim \frac{|S^{d-1}|}{d} \varepsilon^{\frac{\alpha(d+1)}{2}} + \mathcal{O} \left(\varepsilon^{\frac{\alpha(d+2)}{2}} \right), \end{aligned}$$

(in the above multiplicative constants were dropped). The above quantity must behave asymptotically like ε at leading order, and so matching exponents gives us

$$\alpha + \frac{d\alpha}{2} = 1 \Leftrightarrow \alpha = \frac{2}{2+d}.$$

In the continuous case, the optimal potentials must thus behave in the first order like $\varepsilon^{\frac{2}{2+d}}$.

There is a belief in the community that there should be some link between quadratically regularised optimal transport and a class of nonlinear partial differential equations known as the porous medium equation on \mathbb{R}^d for index $m = 2$ (see e.g. Lavenant et al. (2018)), i.e., the equation

$$\frac{\partial u}{\partial t} = \Delta(u^m),$$

where $u = u(x, t)$ and with an initial condition on u at time $t = 0$. Starting from a Dirac mass of integral \mathbf{m} at the origin, the solution of the porous medium equation for $m = 2$ is given by the Barenblatt-Prattle formula (Vázquez, 2007):

$$u(x, t) = \max \left\{ 0, t^{-\frac{d}{2+d}} \left(\mathbf{m} - \frac{1}{4(d+2)} \frac{\|x\|^2}{t^{\frac{2}{2+d}}} \right) \right\}.$$

or, rewriting terms,

$$u(x, t) = \max \left\{ 0, t^{-1} \left(\mathbf{m} t^{\frac{2}{2+d}} - \frac{1}{4(d+2)} \|x\|^2 \right) \right\}.$$

As the porous medium equation conserves mass, the integral of $u(x, t)$ over \mathbb{R}^d remains \mathbf{m} . A key property of the porous medium equation which distinguishes it from the (linear) heat equation is that the solution remains compactly supported. As is evident from e.g. (9), this same property applies to the transport plans derived from quadratically regularised optimal transport.

Perhaps closer to the theory of optimal transport, the porous medium equation of index m can also be understood as the 2-Wasserstein gradient flow of the Tsallis entropy of order m (see for example, the discussion in Peyré (2015)). The Tsallis entropy generalises the Gibbs entropy: for $m = 1$, one recovers the Gibbs entropy, while for $m = 2$ it corresponds to the squared L_2 norm of the density. It is remarkable that the squared L_2 norm is the functional that generates the porous medium equation as Wasserstein gradient flow, which is also the regularising functional used in quadratically regularised optimal transport exhibiting analogous sparsity and scaling behaviour. Furthermore in the entropy regularised setting where $m = 1$, optimal transport enjoys the celebrated connection to a theory of large deviations for Brownian motions and the Schrödinger problem (Léonard, 2013). One interesting theoretical question would be whether similar connections could hold in more general cases, e.g. $m > 1$.

Although our work does not formally establish the existence of such a connection, it is interesting that the same types of exponents appear and that the solution of the porous medium equation is so close in form to the solution of the quadratically regularised optimal transport problem.

3 Results

3.1 Application: manifold learning with heteroskedastic noise

We investigate application of bistochastic projections in Frobenius norm of the linear kernel (which from now on we refer to as the *QOT kernel*) in the setting of a one-dimensional manifold embedded in a high-dimensional ambient space, subjected to noise of varying intensity: this is the setting discussed in Section 2.2. Such a setting may occur for instance in single-cell RNA-sequencing data, where the noise level of cellular gene expression profiles may be determined by factors such as the number of reads sequenced for that cell Landa, Coifman, and Kluger (2021).

We generate synthetic data shown in Figure 1 comprised of $N = 10^3$ points, $\{x_i\}_{i=1}^N$ evenly spaced along the closed curve parameterised by

$$\begin{bmatrix} x(t) \\ y(t) \\ z(t) \end{bmatrix} = \begin{bmatrix} \cos(t)(0.5 \cos(6t) + 1) \\ \sin(t)(0.4 \cos(6t) + 1) \\ 0.4 \sin(6t) \end{bmatrix}, \quad t \in [0, 2\pi].$$

We then randomly construct an orthogonal matrix $R \in \mathbb{R}^{100 \times 3}$, i.e. $R^\top R = I$. Each point $x_i \in \mathbb{R}^3$ is then linearly embedded in the 100-dimensional ambient space with additive noise via $\hat{x}_i = Rx_i + \eta_i$: the noise model we use is

$$\eta_i = \frac{Z_i}{\|Z_i\|} \rho(\theta), \quad 1 \leq i \leq N; \quad \rho(\theta) = 0.05 + 0.95 \frac{1 + \cos(6\theta)}{2},$$

where Z_i follows the standard Gaussian distribution in \mathbb{R}^{100} . In order to eliminate the effect of scaling on the spread parameter ε , we normalise our input data so that $N^{-2} \sum_{i,j=1}^N \|\hat{x}_i - \hat{x}_j\|^2 = 1$. Given the noisy high-dimensional dataset $\{\hat{x}_i\}_{i=1}^N$, we construct affinity matrices using a suite of methods, each with a range of parameter values:

- Bistochastic projection in Frobenius norm (QOT): $\varepsilon \in [10^{-2}, 10^2]$ (logarithmic spacing)
- Bistochastic projection in relative entropy (EOT): (Landa, Coifman, and Kluger, 2021): $\varepsilon \in [10^{-2}, 10^2]$ (logarithmic spacing)
- k -NN with Gaussian edge weights (Belkin and Niyogi, 2003): Symmetrised k -NN affinities with k ranging from 1 to 50 and edge weights $\exp(-\|x_i - x_j\|^2/\varepsilon)$, with ε in same range as EOT.
- Gaussian kernel (Belkin and Niyogi, 2003): dense affinity matrices with edge weights defined by $\exp(-\|x_i - x_j\|^2/\varepsilon)$ for ε in the same range as EOT.
- MAGIC (Van Dijk et al., 2018): Number of neighbours k in the same range as for k -NN.

In Figure 1(a, b), we show the clean, low-dimensional data and the noisy, high-dimensional data projected onto its first three principal components. We next investigate the spectral properties of the various affinity matrix constructions from the noisy high-dimensional data. For a (weighted) affinity matrix W computed by one of the methods we consider, we first row-normalise W to form \bar{W} :

$$\bar{W} = D^{-1}W, \quad D = \text{diag}(W\mathbf{1}).$$

The spectral decomposition of the corresponding (weighted, random-walk normalised) Laplacian $\bar{L} = I - \bar{W}$ is then computed, yielding eigenvalues $\lambda_N \geq \lambda_{N-1} \geq \dots \geq \lambda_1 = 0$ and corresponding right-eigenvectors v_N, \dots, v_1 . The leading eigenvector λ_1 is trivial and so the ℓ -dimensional *eigenmap embedding* for $\ell = 1, \dots, N - 1$ is then the mapping

$$x_i \mapsto (v_2(x_i), v_3(x_i), \dots, v_{\ell+1}(x_i)).$$

We construct a reference graph from the clean 3-dimensional data $\{x_i\}_{i=1}^N$ using k -nearest neighbours with $k = 3$ and compute from its Laplacian reference eigenvectors $\{v_i^{\text{ref}}\}_{i=2}^N$. Since the clean data are evenly spaced, this gives a perfect circle in the first two non-trivial components (Figure 1(e)).

We reason that affinity matrix constructions that are best able to extract latent low-dimensional structure from the noisy, high-dimensional data should have leading Laplacian eigenspaces that are closer to those of the reference Laplacian. To quantitatively measure agreement of eigenspaces, we compute the

principal angle (Knyazev and Argentati, 2002) between the subspaces spanned by the 10 leading non-trivial eigenvectors: i.e. $\text{span}\{v_2, \dots, v_{11}\}$ and $\text{span}\{v_2^{\text{ref}}, \dots, v_{11}^{\text{ref}}\}$. Figure 1(c) summarises these results. It is clear that the graph constructions obtained using the Epanechnikov and Gaussian kernels perform the worst overall – there are no parameter settings for which these methods perform well. This effect can be seen also in Figure 1(d), where the best embeddings in the top two non-trivial eigenvectors of these kernels exhibit clear lobes that arise from the effect of non-uniform noise. Methods based on k -nearest neighbours do significantly better on the other hand: k -NN and MAGIC perform comparably, with the key distinction that MAGIC has the capability of automatically adapting the effective bandwidth across regions of the dataset (and hence does not depend on an ε parameter), while k -NN uses a universal edge weight bandwidth ε that is tuned along with the number of neighbours k .

Among the methods we consider, we find that bistochastic projections with respect to the Frobenius norm (QOT) and the relative entropy (EOT) perform best. This agrees with the observations of Section 2.2 and in Landa, Coifman, and Kluger (2021) – the process of bistochastic projection is able to remove the effect of the heteroskedastic noise. We find further bistochastic projection in the Frobenius norm improves upon the relative entropy in several respects: the best embedding obtained is slightly better than in the case of the relative entropy both visually and in terms of the eigenspaces. More importantly, projection in Frobenius norm yields good spectral agreement for a large range of ε values, spanning over two orders of magnitude. On the other hand, the relative entropy is much more sensitive to its parameter, yielding comparable results only within a narrow range of ε values. We remark that since we plot on a log-scale, our conclusions hold regardless of scale differences in ε between methods.

To further illustrate the difference between the choice of bistochastic projection, we consider the problem of interpolating between two distributions supported on the noisy spiral (see Figure 1(f)). For each method, we consider the best value of ε found previously in terms of eigenspaces. From a bistochastic affinity matrix W we form the Laplacian $L = I - W$ and its corresponding heat kernel $K = e^{-tL}$; we choose $t = 5$. A family of interpolating distributions is produced by solving a Sinkhorn barycenter problem (Peyré, Cuturi, et al., 2019) using K as the reference heat kernel (Solomon et al., 2015). We find that the interpolated distributions for the EOT kernel shows evidence of short-circuiting: this is likely due to the dense nature of the underlying weighted graph, allowing for connections between parts of the manifold that are far apart. On the other hand, the QOT kernel yields interpolations that respect the underlying geometry. This is further evidence that bistochastic projections in Frobenius norm are better suited to downstream applications.

In Figure 1(g) we consider the effect of linear dimensionality reduction via PCA, a pre-processing step that is used ubiquitously when dealing with data of even moderately high dimension (Van Dijk et al., 2018; Schiebinger et al., 2019; Zass and Shashua, 2006; Gorin et al., 2022). We calculate PCA projections of the noisy data ranging from $d = 3$ to $d = 100$ (i.e. full) dimensions. For the optimal choice of parameter ε found previously, we show the Laplacian eigenmap embedding of the QOT kernel computed on each PCA projection. We do the same using k -NN for $k = 25$ and a Gaussian bandwidth of 1.0. We find that k -NN performance progressively degrades as the number of principal components is increased, and even when $d = 3$ the embedding exhibits irregularities. On the other hand, for a fixed value of ε the QOT kernel achieves excellent performance across the full range of dimensionality reduction. This supports the results of Section 2.2.1, that bistochastic kernel projections are robust to high-dimensional settings. In this simple case PCA does not affect the performance of the QOT kernel significantly, however in the case of an additive heteroskedastic noise model we note that preprocessing by PCA could impede the robustness as it modifies the contamination of pairwise distances.

Finally, we remark on the relevance of taking the bistochastic projection of the *linear* kernel. As mentioned in Section 1.2.5, the Gaussian kernel is the natural one (i.e. the one that corresponds to the Euclidean geometry) for taking information projections, while the linear kernel is the natural one for Frobenius projections. In the context of the computational example we consider here, in Figure 6(a) we show the performance (measured in terms of subspace angle, as previously) achieved for Frobenius projection of the linear kernel $-C/\varepsilon$ and the Gaussian kernel $\exp(-C/\varepsilon)$. We observe that projecting the RBF kernel results in worse performance than the linear kernel for ε small. For ε large they begin to coincide, reflecting the fact that $\exp(-C/\varepsilon) \approx 1 - C/\varepsilon$ for $\varepsilon \gg 1$.

3.2 Application: spectral clustering

We consider spectral clustering (von Luxburg, 2007), a problem which is closely related to – but distinct from – manifold learning. This problem was studied by Zass and Shashua, 2006, in which the setting considered was that of finding the bistochastic projection in Frobenius norm of an *arbitrary* affinity

matrix. On the other hand, our insight is that projection of the linear kernel (or equivalently, minus the matrix of pairwise distances) corresponds to the natural Euclidean space, and projecting a different kernel (e.g. the Gaussian kernel, as in (Zass and Shashua, 2006)) implicitly assumes a mapping first to a RKHS before taking the projection. Furthermore, as observed by Landa, Coifman, and Kluger, 2021 it is important to project onto the set of *hollow* bistochastic matrices in order to ensure the robustness property discussed in Section 2.2.

We consider a mixture of $k = 3$ Gaussians, $\mathcal{N}(\mu_i, \sigma_i), 1 \leq i \leq 3$ with 250 points sampled from each mixture component. We choose

$$\mu_1 = \begin{bmatrix} 0 \\ 1 \\ \mathbf{0}^{d-2} \end{bmatrix} \mu_2 = \begin{bmatrix} \sin(2\pi/3) \\ \cos(2\pi/3) \\ \mathbf{0}^{d-2} \end{bmatrix} \mu_3 = \begin{bmatrix} \sin(-2\pi/3) \\ \cos(-2\pi/3) \\ \mathbf{0}^{d-2} \end{bmatrix}.$$

and $\sigma_1 = 0.3, \sigma_2 = 0.6, \sigma_3 = 1.0$. For visualisation purposes, we first set $d = 10$ and compute affinity matrices using QOT, EOT and k -NN with Gaussian edge weights. For each method we take the best value of ε found in a parameter sweep in $\varepsilon \in [10^{-2}, 10^2]$ and we fix $k = 25$ for the k -NN method. In Figure 2(a-c) we show the weighted graphs corresponding to each affinity matrix construction: the sparse nature of the QOT graph is visually discernible. On the other hand, the EOT graph contains many low-weight edges and the k -NN graph contains many edges between clusters.

For a less subjective assessment of the affinity matrix constructions, for each affinity matrix W we form the corresponding symmetrically normalised Laplacian $L = I - D^{-1/2}WD^{-1/2}$ and compute its second (Fiedler) eigenvalue-eigenvector pair (λ_2, v_2) . This can be interpreted in terms of a minimal graph cut problem, where v_2 partitions vertices by its sign, and λ_2 measures the connectivity across the cut (von Luxburg, 2007). As we show in the inset plots, the Fiedler vector v_2 of the QOT kernel cleanly separates out component 1 from components 2 and 3 and achieves the lowest value of λ_2 . On the other hand, both the EOT and k -NN kernels produce Fiedler vectors that are less clean, and correspondingly higher values of λ_2 suggest stronger connections between clusters.

Next we consider a much higher dimensional setting, $d = 250$. Constructing affinity matrices using QOT, EOT and k -NN with Gaussian edge weights, we perform a parameter sweep for $\varepsilon \in [10^{-2}, 10^2]$ and report spectral clustering performance in terms of the normalised mutual information (NMI). In Figure 2(e) we see that both QOT and EOT far outperform k -NN as expected, but also that QOT outperforms EOT by a significant margin. As in the manifold learning example, we considered the effect of a PCA preprocessing step in Figure 2(f). Choosing ε to be the best value found for each method previously, we find that QOT is robust to the number of principal components used. On the other hand, both EOT and k -NN are sensitive to the number of principal components chosen: k -NN performs reasonably only for the smallest number of components considered ($n = 5$) and worse than QOT for any tested value of its parameter ε . On the other hand, performance of EOT in fact degraded as the number of principal components decreased, potentially related to the poor spectral properties as a result of the dense nature of the affinity matrices.

Finally, we illustrate in Figure 6(b) the importance of ensuring a *hollow* projection, as opposed to a *fat* projection where no constraint is imposed on the diagonal of the projected affinity matrix. Intuitively, as the parameter $\varepsilon \rightarrow 0$ the solution to the non-hollow projection will concentrate on the diagonal. While there is no effect in the continuous setting, for discrete data the unconstrained projection may lead to affinities that are degenerate, i.e. an affinity matrix where some points only have self-connections. Enforcing the hollow projection prevents this from occurring, as well as allowing one to utilise the robustness results of Section 2.2 for high-dimensional noise.

3.3 Application: single cell RNA sequencing data

Datasets of high-throughput measurements made from biological systems are naturally high dimensional and usually subject to significant noise, both biological and technical. Single cell RNA sequencing datasets typically comprise of on the order of $10^3 - 10^6$ cells and have an ambient dimensionality on the order of 10^4 , or the number of expressed genes in an organism. In many cases, the measured cells are captured along a continuous biological process such as development. The high-dimensional cell state data can be thought of as an embedded lower dimensional manifold whose intrinsic geometry captures biological details Moon et al., 2018; Van Dijk et al., 2018.

We consider one such dataset, originally published in La Manno et al. (2018) that captures the spectrum of cell states across the development of mouse hippocampus. Starting from a sample of 5,000 cells we apply the standard filtering and pre-processing pipeline (filter out low expression cells and genes,

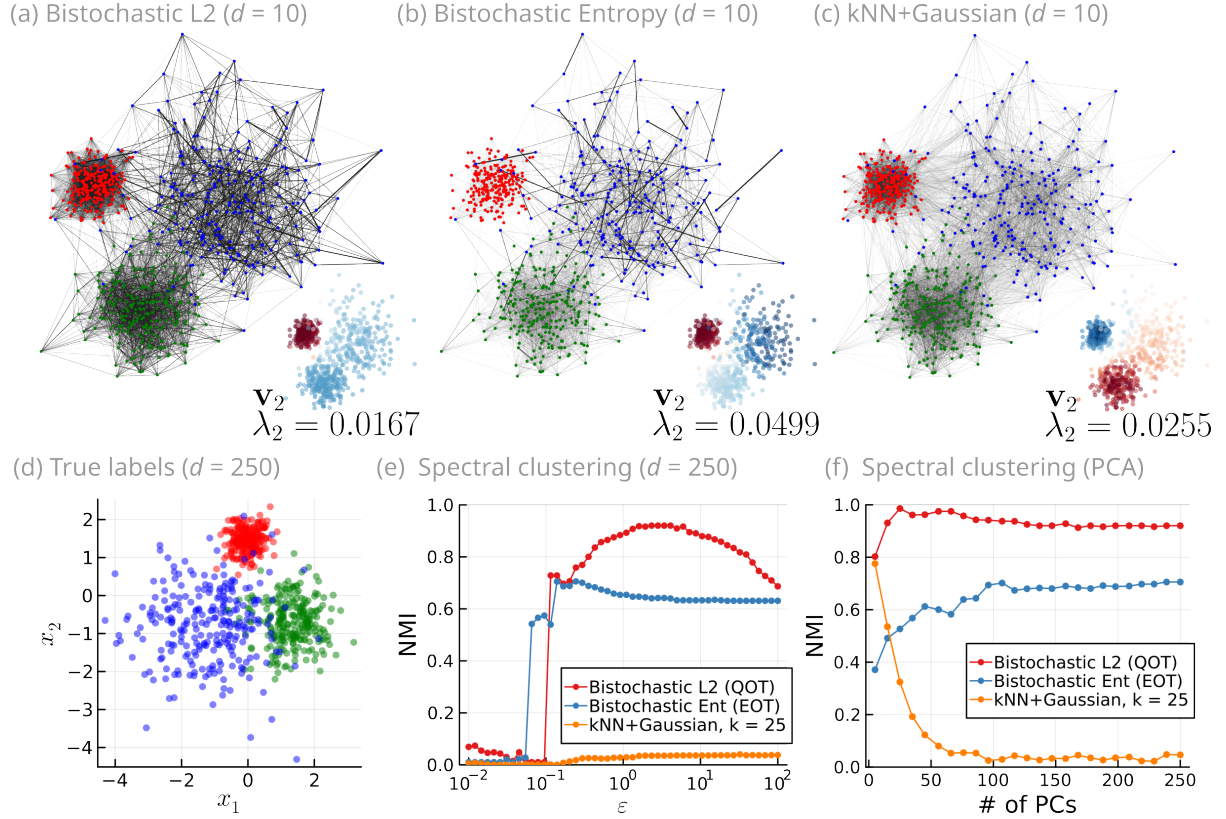


Figure 2: **Gaussian mixture model.** (a-c) $N = 750$ points sampled from a mixture of 3 Gaussians (250 points each) in $d = 10$ dimensions, coloured by their true labels, with weighted graphs corresponding to the QOT, EOT and k -NN kernels respectively. Inset: the values of the second smallest eigenvector and eigenvalue of the affinity matrix. (d) $N = 750$ sampled from a mixture of 3 Gaussians (250 points each) in $d = 100$ dimensions, coloured by their true labels. (e-f) Performance (measured in terms of the normalised mutual information) of each kernel (bistochoastic L2, bistochoastic entropic, k -NN + Gaussian) for the task of spectral clustering, (e) for different values of the parameter ε and (f) for different numbers of principal components with a fixed value of the parameter ε .

normalise reads per cell, $\log(x + 1)$ transformation, filter for highly variable genes and standardisation). This leads to a 5000×2239 matrix of normalised cell-by-gene expression values. We computed affinity matrices using QOT and EOT, as well as k -NN with unit edge weights. For each affinity matrix, we transformed the cells into a 10-dimensional spectral embedding. In the spectral embedding coordinates we calculated the squared distance of each cell to an origin cell which was selected based on origin-cell probabilities calculated by La Manno et al. (2018, Figure 3) from RNA velocity reconstructions.

We show in Figure 3 on t -SNE coordinates the distance-to-origin cell as measured in the Laplacian eigenmap embeddings calculated based on the QOT and EOT affinity matrices, as well as the k -NN adjacency matrix. We observe that the QOT kernel produces an embedding in which the ends of branches of developmental lineages are distant from the origin cell. This is in agreement with the end-state predictions calculated by La Manno et al. (2018, Figure 3) from RNA velocity reconstructions. On the other hand, the EOT and k -NN kernel constructions miss certain lineages.

Despite being a staple of single cell data analysis pipelines (Moon et al., 2018; La Manno et al., 2018), the use of k -nearest neighbours for constructing affinity matrices has rarely been questioned (Gorin et al., 2022). Our findings suggest that construction of affinity matrices by k -NN may be suboptimal for high-dimensional data, a regime in which we find the QOT construction to perform favourably.

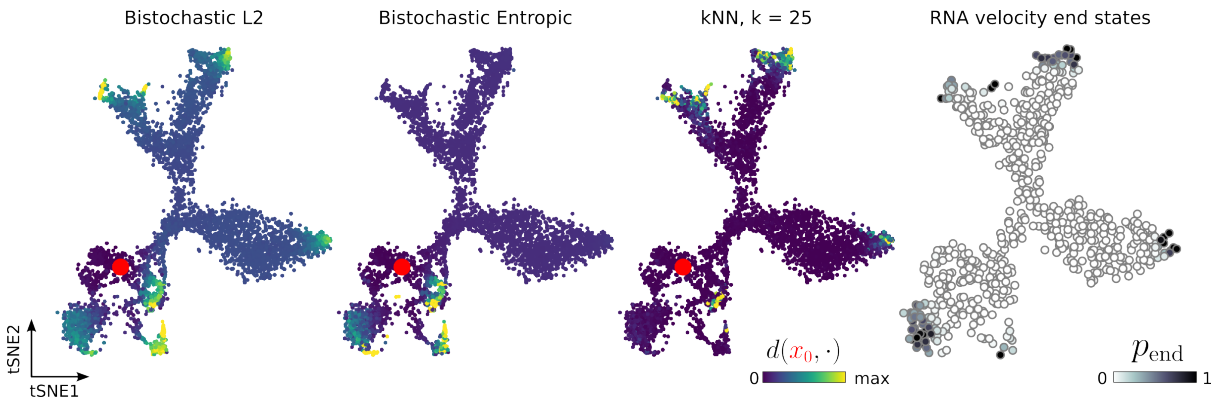


Figure 3: **Single cell RNA sequencing dataset.** Sub-sampled dentate gyrus dataset (La Manno et al., 2018) (5000 cells, 2239 dimensions) visualised in t -SNE coordinates from the original publication. Left: coloured by squared distance from origin cell (red) measured in terms of the 10-dimensional spectral embedding, for QOT, EOT and k -NN affinity matrix constructions respectively. Right: terminal cell states predicted by (La Manno et al., 2018) using RNA velocity estimates.

4 Conclusion and open questions

Our work opens the door for further applications and analysis of the bistochastic projection of affinity matrices in the Frobenius norm. Understanding finely the relationship between the porous medium equation and regularised optimal transport one concrete interesting theoretical problem; we only strengthen the apparent parallel in Section 2.5. The understanding might further help explain why the methods performs well and more precisely help identify the weaknesses. Furthermore, determining the limiting operators that arise from this scheme for other settings is still an open question – could one derive finer results on the potentials or further exploit the metric projection property?

Finally, even though first results are given in that direction in Section 2.2, providing a comprehensive, quantitative rationale for the overperformance observed in Section 3 would be welcome. A finer description of the finite sample case would be valuable. Also, understanding when the method is not suitable would also be important for a controlled, widespread use.

Acknowledgements

S. Zhang acknowledges support from an Australian Government Research Training Program Scholarship and an Elizabeth and Vernon Puzey Scholarship. G. Mordant acknowledges the support of the DFG within CRC1456-A04. G. Schiebinger was supported by a MSHR Scholar Award, a CASI from the Burroughs Wellcome Fund and a CIHR Project Grant.

References

- Bao, Han and Shinsaku Sakaue (2022). “Sparse Regularized Optimal Transport with Deformed q -Entropy”. In: *Entropy* 24.11, p. 1634.
- Belkin, Mikhail and Partha Niyogi (2003). “Laplacian eigenmaps for dimensionality reduction and data representation”. In: *Neural computation* 15.6, pp. 1373–1396.
- Belkin, Mikhail, Partha Niyogi, and Vikas Sindhwani (2006). “Manifold regularization: A geometric framework for learning from labeled and unlabeled examples.” In: *Journal of machine learning research* 7.11.
- Bhatia, Rajendra (2013). *Matrix analysis*. Vol. 169. Springer Science & Business Media.
- Cai, Deng et al. (2008). “Non-negative matrix factorization on manifold”. In: *2008 eighth IEEE international conference on data mining*. IEEE, pp. 63–72.
- Carlier, Guillaume, Victor Chernozhukov, and Alfred Galichon (2016). “Vector quantile regression: an optimal transport approach”. In.
- Coifman, Ronald R and Stéphane Lafon (2006). “Diffusion maps”. In: *Applied and computational harmonic analysis* 21.1, pp. 5–30.
- Coifman, Ronald R et al. (2005). “Geometric diffusions as a tool for harmonic analysis and structure definition of data: Diffusion maps”. In: *Proceedings of the national academy of sciences* 102.21, pp. 7426–7431.
- Crane, Keenan, Clarisse Weischedel, and Max Wardetzky (2013). “Geodesics in heat: A new approach to computing distance based on heat flow”. In: *ACM Transactions on Graphics (TOG)* 32.5, pp. 1–11.
- Cuturi, Marco (2013). “Sinkhorn distances: Lightspeed computation of optimal transport”. In: *Advances in neural information processing systems* 26.
- Ding, Tianjiao et al. (2022). “Understanding doubly stochastic clustering”. In: *International Conference on Machine Learning*. PMLR, pp. 5153–5165.
- Essid, Montacer and Justin Solomon (2018). “Quadratically regularized optimal transport on graphs”. In: *SIAM Journal on Scientific Computing* 40.4, A1961–A1986.
- Feydy, Jean et al. (2019). “Interpolating between optimal transport and mmd using sinkhorn divergences”. In: *The 22nd International Conference on Artificial Intelligence and Statistics*. PMLR, pp. 2681–2690.
- Gorin, Gennady et al. (2022). “RNA velocity unraveled”. In: *PLOS Computational Biology* 18.9, e1010492.
- Grigoryan, Alexander (2009). *Heat kernel and analysis on manifolds*. Vol. 47. American Mathematical Soc.
- Gulrajani, Ishaan et al. (2017). “Improved training of wasserstein gans”. In: *Advances in neural information processing systems* 30.
- Hallin, Marc and Gilles Mordant (2022). “Center-Outward Multiple-Output Lorenz Curves and Gini Indices a measure transportation approach”. In: *arXiv preprint arXiv:2211.10822*.
- Hallin, Marc, Gilles Mordant, and Johan Segers (2021). “Multivariate goodness-of-fit tests based on Wasserstein distance”. In.
- Hallin, Marc et al. (2021). “Distribution and quantile function, ranks and signs in dimension d : A measure transportation approach”. In: *The Annals of Statistics* 49.2, pp. 1139–1165.
- Hein, Matthias and Jean-Yves Audibert (2005). “Intrinsic dimensionality estimation of submanifolds in \mathbb{R}^d ”. In: *Proceedings of the 22nd international conference on Machine learning*, pp. 289–296.
- Hundrieser, Shayan, Thomas Staudt, and Axel Munk (2022). “Empirical optimal transport between different measures adapts to lower complexity”. In: *arXiv preprint arXiv:2202.10434*.
- Hundrieser, Shayan et al. (2023). “Empirical Optimal Transport under Estimated Costs: Distributional Limits and Statistical Applications”. In: *arXiv preprint arXiv:2301.01287*.
- Knyazev, Andrew V and Merico E Argentati (2002). “Principal angles between subspaces in an A-based scalar product: algorithms and perturbation estimates”. In: *SIAM Journal on Scientific Computing* 23.6, pp. 2008–2040.
- Kollo, Tõnu and Dietrich von Rosen (2005). *Advanced multivariate statistics with matrices*. Mathematics and Its Applications. Springer.
- La Manno, Gioele et al. (2018). “RNA velocity of single cells”. In: *Nature* 560.7719, pp. 494–498.
- Landa, Boris and Xiuyuan Cheng (2022). “Robust inference of manifold density and geometry by doubly stochastic scaling”. In: *arXiv preprint arXiv:2209.08004*.
- Landa, Boris, Ronald R Coifman, and Yuval Kluger (2021). “Doubly stochastic normalization of the gaussian kernel is robust to heteroskedastic noise”. In: *SIAM journal on mathematics of data science* 3.1, pp. 388–413.

- Lavenant, Hugo et al. (2018). “Dynamical optimal transport on discrete surfaces”. In: *ACM Transactions on Graphics (TOG)* 37.6, pp. 1–16.
- Lavenant, Hugo et al. (2021). “Towards a mathematical theory of trajectory inference”. In: *arXiv preprint arXiv:2102.09204*.
- Léonard, Christian (2013). “A survey of the Schrödinger problem and some of its connections with optimal transport”. In: *ArXiv:1308.0215*.
- Lévy, Bruno (2006). “Laplace-beltrami eigenfunctions towards an algorithm that” understands” geometry”. In: *IEEE International Conference on Shape Modeling and Applications 2006 (SMI'06)*. IEEE, pp. 13–13.
- Lim, Derek, René Vidal, and Benjamin D Haeffele (2020). “Doubly stochastic subspace clustering”. In: *arXiv preprint arXiv:2011.14859*.
- Lorenz, Dirk A, Paul Manns, and Christian Meyer (2021). “Quadratically regularized optimal transport”. In: *Applied Mathematics & Optimization* 83.3, pp. 1919–1949.
- Malik, John et al. (2019). “Connecting dots: from local covariance to empirical intrinsic geometry and locally linear embedding”. In: *Pure and Applied Analysis* 1.4, pp. 515–542.
- Marshall, Nicholas F and Ronald R Coifman (2019). “Manifold learning with bi-stochastic kernels”. In: *IMA Journal of Applied Mathematics* 84.3, pp. 455–482.
- Moon, Kevin R et al. (2018). “Manifold learning-based methods for analyzing single-cell RNA-sequencing data”. In: *Current Opinion in Systems Biology* 7, pp. 36–46.
- Mordant, Gilles and Johan Segers (2022). “Measuring dependence between random vectors via optimal transport”. In: *Journal of Multivariate Analysis* 189, p. 104912.
- Nies, Thomas Giacomo, Thomas Staudt, and Axel Munk (2021). “Transport dependency: Optimal transport based dependency measures”. In: *arXiv preprint arXiv:2105.02073*.
- Peyré, Gabriel (2015). “Entropic approximation of Wasserstein gradient flows”. In: *SIAM Journal on Imaging Sciences* 8.4, pp. 2323–2351.
- Peyré, Gabriel, Marco Cuturi, et al. (2019). “Computational optimal transport: With applications to data science”. In: *Foundations and Trends® in Machine Learning* 11.5-6, pp. 355–607.
- Reuter, Martin, Franz-Erich Wolter, and Niklas Peinecke (2006). “Laplace–Beltrami spectra as ‘Shape-DNA’ of surfaces and solids”. In: *Computer-Aided Design* 38.4, pp. 342–366.
- Saul, Lawrence K and Sam T Roweis (2000). “An introduction to locally linear embedding”. In: *unpublished. Available at: <http://www.cs.toronto.edu/~roweis/lle/publications.html>*.
- Schiebinger, Geoffrey et al. (2019). “Optimal-transport analysis of single-cell gene expression identifies developmental trajectories in reprogramming”. In: *Cell* 176.4, pp. 928–943.
- Schmitzer, Bernhard (2019). “Stabilized sparse scaling algorithms for entropy regularized transport problems”. In: *SIAM Journal on Scientific Computing* 41.3, A1443–A1481.
- Solomon, Justin et al. (2015). “Convolutional wasserstein distances: Efficient optimal transportation on geometric domains”. In: *ACM Transactions on Graphics (ToG)* 34.4, pp. 1–11.
- Tenenbaum, Joshua B, Vin de Silva, and John C Langford (2000). “A global geometric framework for nonlinear dimensionality reduction”. In: *science* 290.5500, pp. 2319–2323.
- Ting, Daniel, Ling Huang, and Michael I Jordan (2010). “An analysis of the convergence of graph Laplacians”. In: *Proceedings of the 27th International Conference on International Conference on Machine Learning*, pp. 1079–1086.
- Torous, William, Florian Gunsilius, and Philippe Rigollet (2021). “An optimal transport approach to causal inference”. In: *arXiv preprint arXiv:2108.05858*.
- Tsybakov, Alexandre (2008). *Introduction to Nonparametric Estimation*. Springer Series in Statistics. Springer New York.
- Van Dijk, David et al. (2018). “Recovering gene interactions from single-cell data using data diffusion”. In: *Cell* 174.3, pp. 716–729.
- Vázquez, Juan Luis (2007). *The porous medium equation: mathematical theory*. Oxford University Press on Demand.
- von Luxburg, Ulrike (2007). “A tutorial on spectral clustering”. In: *Statistics and computing* 17, pp. 395–416.
- von Luxburg, Ulrike, Mikhail Belkin, and Olivier Bousquet (2008). “Consistency of spectral clustering”. In: *The Annals of Statistics*, pp. 555–586.
- Wu, Hau-Tieng and Nan Wu (2018). “Think globally, fit locally under the manifold setup: Asymptotic analysis of locally linear embedding”. In: *The Annals of Statistics* 46.6B, pp. 3805–3837.
- Yu, Yi, Tengyao Wang, and Richard J Samworth (2015). “A useful variant of the Davis–Kahan theorem for statisticians”. In: *Biometrika* 102.2, pp. 315–323.

- Zass, Ron and Amnon Shashua (2006). “Doubly stochastic normalization for spectral clustering”. In: *Advances in neural information processing systems* 19.
- Zhang, Stephen et al. (2021). “Optimal transport analysis reveals trajectories in steady-state systems”. In: *PLoS computational biology* 17.12, e1009466.
- Zhang, Stephen Y (2021). “A unified framework for non-negative matrix and tensor factorisations with a smoothed Wasserstein loss”. In: *Proceedings of the IEEE/CVF International Conference on Computer Vision*, pp. 4195–4203.
- Zhang, Zhenyue and Hongyuan Zha (2004). “Principal manifolds and nonlinear dimensionality reduction via tangent space alignment”. In: *SIAM journal on scientific computing* 26.1, pp. 313–338.

A Supplementary theory

A.1 General regularised optimal transport

For simplicity we will restrict our focus to discrete measures.

Definition 1 (Regularized optimal transport). *Consider a two discrete probability measures α, β supported on n and m points respectively. Recall that $\Pi(\alpha, \beta)$ denotes the set of couplings between α and β . Consider additionally a smooth convex function $\Omega : \mathbb{R}^{n \times m} \rightarrow \mathbb{R}$ and a cost matrix $C \in \mathbb{R}^{n \times m}$. Then, for $\varepsilon > 0$, the optimisation problem*

$$\min_{\pi \in \Pi(\alpha, \beta)} \langle C, \pi \rangle + \varepsilon \Omega(\pi)$$

is called a regularised optimal transport problem.

Lemma 3 (Dual of regularized optimal transport). *Consider the regularised optimal transport problem with smooth, convex regulariser Ω .*

$$\min_{\pi \in \Pi(\alpha, \beta)} \langle C, \pi \rangle + \varepsilon \Omega(\pi)$$

Then, the corresponding dual problem is

$$\sup_{u, v} -\langle u, \alpha \rangle - \langle v, \beta \rangle - \varepsilon \inf_{\rho \geq 0} \Omega^* \left(-\frac{C + u \oplus v - \rho}{\varepsilon} \right).$$

where Ω^* is the Legendre transform of Ω in its argument.

In the setting of optimal transport with a quadratic regularisation, we choose

$$\Omega(\pi) = \frac{1}{2} \|\pi\|_{\mu \otimes \nu}^2 = \frac{1}{2} \left\langle \frac{d\pi}{d\mu \otimes d\nu}, \pi \right\rangle.$$

A straightforward computation reveals that

$$\Omega^*(\rho) = \frac{1}{2} \|\rho(\mu \otimes \nu)\|_{\mu \otimes \nu}^2.$$

It follows that the dual for the quadratically regularised optimal transport problem is

$$\sup_{u, v} \langle u, \alpha \rangle + \langle v, \beta \rangle - \frac{1}{2\varepsilon} \|[u \oplus v - C]_+(\mu \otimes \nu)\|_{\mu \otimes \nu}^2.$$

Lemma 4 (Dual of hollow regularized optimal transport). *Consider the hollow regularised optimal transport problem with smooth, convex regulariser Ω , denoting by Ho the set of matrices with zero diagonal:*

$$\inf_{\pi \in \Pi(\alpha, \beta) \cap \text{Ho}} \langle C, \pi \rangle + \varepsilon \Omega(\pi)$$

Then, the corresponding dual problem is

$$\sup_{u, v, D} -\langle u, \alpha \rangle - \langle v, \beta \rangle - \varepsilon \inf_{\rho \geq 0} \Omega^* \left(-\frac{C + D + u \oplus v - \rho}{\varepsilon} \right),$$

where D is in the set of diagonal matrices.

Proof. The Lagrange formulation of the problem reads

$$\inf_{\pi \geq 0} \sup_{u \in \mathbb{R}^n, v \in \mathbb{R}^m, D} \langle C, \pi \rangle + \varepsilon \Omega(\pi) + \langle \alpha - \pi \mathbf{1}, u \rangle + \langle \beta - \pi^\top \mathbf{1}, v \rangle + \langle D, \pi \rangle,$$

where the optimisation for D occurs on the set of diagonal matrices. On thus gets the classical dual formulation for the modified cost matrix. \square

Remark 7 (A note on the case of empirical measures). In the discrete setting where $\mu = N^{-1} \sum_i \delta_{x_i}, \nu = M^{-1} \sum_j \delta_{y_j}$, one has $\frac{\varepsilon}{2} \|\pi\|_{\mu \otimes \nu}^2 = \frac{\varepsilon N^2}{2} \|\pi\|_{\mathbf{1} \otimes \mathbf{1}}^2$.

A.2 Details on generalised bistochastic information projections

For a parameter $q \in [0, 1)$, a deformed analogue of the entropy, the q -entropy, is defined by Bao and Sakaue (2022) as $\phi(x) = \frac{1}{2-q}(x \log_q x - x)$, $x \geq 0$ where the q -analogues of the exponential and its inverse are defined for $q \in [0, 1)$ as

$$\begin{aligned}\exp_q(x) &= [1 + (1-q)x]_+^{1/(1-q)}, \\ \log_q(x) &= (1-q)^{-1}(x^{1-q} - 1).\end{aligned}$$

Since ϕ is differentiable and convex on its domain, it generates a Bregman divergence on matrices with the formula

$$\Phi(A|B) = \frac{1}{2-q} \sum_{i,j} \left[A_{ij} \log_q A_{ij} - A_{ij} \log_q B_{ij} - A_{ij} B_{ij}^{1-q} + B_{ij}^{2-q} \right].$$

It is straightforward to verify that as $q \rightarrow 1$ one recovers the standard exponential and logarithm, and thus Φ becomes the KL divergence. When $q = 0$, corresponding to the squared Frobenius norm, we have that $\phi(x) = x^2/2 - x + \iota(x \geq 0)$, $\phi^*(u) = \frac{1}{2}[1+u]_+^2$, $\nabla\phi^*(u) = [1+u]_+$ and so

$$\Phi(A|B) = \frac{1}{2} \|A_{ij} - B_{ij}\|_2^2.$$

Consider then the generalised Bregman projection problem

$$\operatorname{argmin}_{A \in \Pi(\mathbf{1}, \mathbf{1})} \varepsilon \Phi^* \left(\frac{-C}{\varepsilon}, \nabla\phi(A) \right) \quad (13)$$

where Φ^* is the Bregman divergence generated by ϕ^* , the convex conjugate of ϕ . When $q \rightarrow 1$, $\phi^*(u) \rightarrow e^u$ and is smooth on its domain, so the objective function is exactly equal to $\varepsilon \Phi(A, \nabla\phi^*(-C/\varepsilon))$. For other cases, however, ϕ^* fails to be smooth and we must consider the problem (13) to avoid loss of information. Expanding the definition of Φ ,

$$\begin{aligned}\varepsilon \Phi^* \left(\frac{-C}{\varepsilon}, \nabla\phi(A) \right) &= \varepsilon \sum_{ij} \phi^*(-C_{ij}/\varepsilon) - \phi^*(\nabla\phi(A_{ij})) - \nabla\phi^*(\nabla\phi(A_{ij}))(-C_{ij}/\varepsilon - \nabla\phi(A_{ij})) \\ &= \varepsilon \sum_{ij} \phi^*(-C_{ij}/\varepsilon) - \phi^*(\nabla\phi(A_{ij})) \\ &\quad + \nabla\phi^*(\nabla\phi(A_{ij}))C_{ij}/\varepsilon + \nabla\phi^*(\nabla\phi(A_{ij}))\nabla\phi(A_{ij}) \\ &= \varepsilon \sum_{ij} \phi^*(-C_{ij}/\varepsilon) + A_{ij}C_{ij}/\varepsilon + \phi(A_{ij}),\end{aligned}$$

Which is, up to a constant, exactly the regularised optimal transport problem. Since ϕ is convex, by the above expansion we see that the problem in A remains convex. In the above, since $A_{ij} \geq 0$, we have that $\nabla\phi \circ \nabla\phi^{-1} = \text{id}$, and also $\phi^*(\nabla\phi(x)) = x\nabla\phi(x) - \phi(x)$.

We remark that when $q = 1$, $\exp(-C/\varepsilon)$ is the well-known Gibbs kernel and for $q \in [0, 1)$ one may write $\exp_q(-C/\varepsilon)$ to be the q -Gibbs kernel (Bao and Sakaue, 2022). However, \exp_q involves a thresholding of the cost matrix and thus is not equivalent to the regularised optimal transport problem. (This is a result of ϕ^* failing to be smooth in such cases.) So, while the general problem is *formally* the projection of the q -Gibbs kernel, it is more precisely understood as being done via the dual formulation.

A.3 Additional lemmas and proofs

In this appendix, we collect some useful lemmas.

Proof. (Proof of Proposition 1) First we establish that projection in the set of hollow bistochastic matrices is invariant with respect to addition of diagonal matrices. Indeed, for a diagonal matrix K ;

$$\min_{\pi \in \mathcal{K}} \sum_{i,j} \pi_{i,j} \tilde{c}_{i,j} + \frac{\varepsilon}{2} \|\pi\|_F^2 = \min_{\pi \in \mathcal{K}} \sum_{i,j} \pi_{i,j} (\tilde{c}_{i,j} + K_{i,j}) + \frac{\varepsilon}{2} \|\pi\|_F^2,$$

as $\pi_{i,i} = 0$. Then, in the error model that we have,

$$\|\tilde{x}_i - \tilde{x}_j\|^2 = \|x_i - x_j\|^2 + 2\langle \tilde{x}_i - \tilde{x}_j, \eta_i - \eta_j \rangle + \|\eta_i\|^2 + \|\eta_j\|^2 - \langle \eta_i, \eta_j \rangle.$$

Note that, for $i \neq j$, by the same arguments as in Landa, Coifman, and Kluger (2021, Lemma 4)

$$2\langle \tilde{x}_i - \tilde{x}_j, \eta_i - \eta_j \rangle - \langle \eta_i, \eta_j \rangle = \mathcal{O}_p(m^{-1/2}).$$

However, when $i = j$

$$\|\tilde{x}_i - \tilde{x}_j\|^2 = \|x_i - x_j\|^2 = 0.$$

One thus has that the noisy cost matrix is the pure cost matrix plus a rank-one perturbation plus a noise matrix E up to adding the lacking diagonal element of the rank-one perturbation. We can thus add the diagonal missing part so that

$$\min_{\pi \in \mathcal{K}} \sum_{i,j} \pi_{i,j} \tilde{c}_{i,j} + \frac{\varepsilon}{2} \|\pi\|_F^2 = \min_{\pi \in \mathcal{K}} \sum_{i,j} \pi_{i,j} (c_{i,j} + \eta_i + \eta_j + E_{i,j}) + \frac{\varepsilon}{2} \|\pi\|_F^2,$$

where $E_{i,j}$ is hollow and $\mathcal{O}_p(m^{-1/2})$. Finally observe that,

$$\sum_{i,j} \pi_{i,j} \eta_i$$

is a constant and independent of the optimal permutation chosen. Therefore, one gets that $W_\varepsilon^{(f)}(\tilde{C}) = W_\varepsilon^{(f)}(C + E)$ and one can use Lemma 2 to deduce the claim. \square

Lemma 5. For $x_0 \in \mathcal{M}$, it holds for r sufficiently small that

$$\begin{aligned} \mathbb{E} [f(X; r) \mathbf{1}\{\|X - \iota(x_0)\| \leq r\}] &= \frac{|S^{d-1}|}{d \operatorname{vol}(\mathcal{M})} f(\iota(x_0); r) r^d \\ &+ \frac{|S^{d-1}|}{d(d+2)} \left(\frac{1}{2 \operatorname{vol}(\mathcal{M})} \Delta f(x_0; r) + \frac{s(x_0) f(x_0; r)}{6 \operatorname{vol}(\mathcal{M})} \right. \\ &\quad \left. + \frac{d(d+2) \omega(x_0) f(x_0; r)}{24 \operatorname{vol}(\mathcal{M})} \right) r^{d+2} \\ &+ \mathcal{O}(f(x_0; r) r^{d+3}). \end{aligned} \quad (14)$$

Proof. This is a slight variation of Lemma B.5 of (Wu and Wu, 2018) for a uniform density and in which the functions are allowed to depend on the parameter r . Because of this modification the asymptotic expansion has been slightly refined. \square

Lemma 6. For fixed $x_0 \in \mathcal{M}$, r sufficiently small and X uniformly distributed on \mathcal{M} under Assumptions 1 and 2, it holds that

$$\begin{aligned} \mathbb{E} (f(X; r) (X - \iota(x_0)) (X - \iota(x_0))^\top \mathbf{1}\{\|X - \iota(x_0)\| \leq r\}) \\ = \frac{|S^{d-1}|}{d(d+2) \operatorname{vol}(\mathcal{M})} f(\iota(x_0); r) r^{d+2} \left(\begin{pmatrix} I_{d \times d} & 0 \\ 0 & 0 \end{pmatrix} + \mathcal{O}(r^2) \right) \end{aligned}$$

Proof. The proof follows along the same lines as Proposition 3.1 in Wu and Wu (2018). \square

Lemma 7. For fixed $x_0 \in \mathcal{M}$, r sufficiently small and X uniformly distributed on \mathcal{M} under Assumptions 1 and 2, it holds that

$$\begin{aligned} \mathbb{E} [f(X; r) e_k^\top (X - \iota(x_0)) (X - \iota(x_0))^\top e_l e_m^\top (X - \iota(x_0)) (X - \iota(x_0))^\top e_n \mathbf{1}\{\|X - \iota(x_0)\| \leq r\}] \\ = \frac{f(\iota(x_0); r)}{(d+4) \operatorname{vol}(\mathcal{M})} r^{d+4} C_{k,l,m,n} + \mathcal{O}(r^{d+5}), \end{aligned}$$

where

$$C_{k,l,m,n} = \int_{S^{d-1}} \langle \iota_* \theta, e_k \rangle \langle \iota_* \theta, e_l \rangle \langle \iota_* \theta, e_m \rangle \langle \iota_* \theta, e_n \rangle d\theta$$

Proof. First set

$$\tilde{B}_r(x_0) := \iota^{-1}(B_r^{\mathbb{R}^p}(\iota(x_0)) \cap \iota(\mathcal{M})).$$

Then, the quantity of interest can be written

$$\mathcal{I} := \frac{1}{\text{vol}(\mathcal{M})} \int_{\tilde{B}_r(x_0)} \langle \iota(y) - \iota(x_0), e_k \rangle \langle \iota(y) - \iota(x_0), e_l \rangle \\ \times \langle \iota(y) - \iota(x_0), e_m \rangle \langle \iota(y) - \iota(x_0), e_n \rangle f(y) dV(y).$$

Recalling that for $(t, \theta) \in [0, \infty) \times S^{d-1}$

$$\begin{aligned} \iota \circ \exp_{x_0}(\theta t) - \iota(x_0) &= \iota_* \theta t + \mathcal{O}(t^2) \\ \tilde{r} &= r + \mathcal{O}(r^3) \\ dV(\exp_{x_0}(\theta t)) &= t^{d-1} + \mathcal{O}(t^{d+1}) \\ f(\exp_{x_0}(\theta t)) &= f(x_0) + \mathcal{O}(t), \end{aligned}$$

it holds that

$$\begin{aligned} \mathcal{I} &= \frac{1}{\text{vol}(\mathcal{M})} \int_{S^{d-1}} \int_0^{\tilde{r}} f(x_0) t^{d+3} \langle \iota_* \theta, e_k \rangle \langle \iota_* \theta, e_l \rangle \langle \iota_* \theta, e_m \rangle \langle \iota_* \theta, e_n \rangle + \mathcal{O}(t^{d+4}) dt d\theta \\ &= \frac{f(x_0)}{\text{vol}(\mathcal{M})(d+4)} r^{d+4} \int_{S^{d-1}} \langle \iota_* \theta, e_k \rangle \langle \iota_* \theta, e_l \rangle \langle \iota_* \theta, e_m \rangle \langle \iota_* \theta, e_n \rangle d\theta + \mathcal{O}(r^{d+5}); \end{aligned}$$

as claimed. \square

Proof of Lemma 1. Using Lemma 5 with $f = 1$, we get that the quantile function of the local distribution of squared distances at x_0 is approximately

$$p \mapsto \left(\frac{p}{|S^{d-1}| d^{-1} \text{vol}(\mathcal{M})^{-1}} \right)^{2/d},$$

so that the duality constraint in the discrete problem is approximately

$$\frac{N+1}{\varepsilon} \sum_{j=0}^N \left(u^*(X_0) + u^*(X_j) - \left(\frac{U_{(j:N)}}{|S^{d-1}| d^{-1} \text{vol}(\mathcal{M})^{-1}} \right)^{2/d} \right)_+ = 1, \quad (15)$$

where $U_{(j:N)}$ is the j -th sorted element of an i.i.d. sample of size N of random variables uniformly distributed on $[0, 1]$ and we take $U_{(0:N)} = 0$. Note that although we write down all N order statistics $U_{(j:N)}$ and the expression for the quantile function is only a good approximation for $p \ll 1$, as long as $u(x_0) + u(X_j)$ is small, only the first few terms will be nonzero.

We get the equivalent problem

$$\frac{N+1}{\varepsilon(N+1)^{2/d}} \kappa_d \sum_{j=0}^N \left(\tilde{u}(x_0) + \tilde{u}(X_j) - U_{(j:N)}^{2/d} \right)_+ = 1, \quad (16)$$

where we have set

$$\tilde{u}(\cdot) = \frac{(N+1)^{2/d}}{\kappa_d} u^*(\cdot).$$

Choose $k^{2/d} < 2\tilde{u} \leq (k+1)^{2/d}$ and plug \tilde{u} (choosing a constant approximation to the potential) as a choice for the potential in (16). It yields,

$$\frac{N+1}{\varepsilon(N+1)^{2/d}} \kappa_d \left[2(k+1)\tilde{u} - \sum_{j=1}^k U_{(j:N)}^{2/d} \right] = 1. \quad (17)$$

Let us turn to the size of the sum in (17). First, basic calculations show that

$$\mathbb{E} \left[\left(U_{(j:N)} \right)^{2/d} \right] = \frac{\Gamma(\frac{2}{d} + j) \Gamma(N+1)}{\Gamma(\frac{2}{d} + N+1) \Gamma(j)},$$

So that understanding the problem (15), even in expectation and for constant potentials is not so easy for $d > 2$.

For $d = 1$, we get

$$\sum_{j=1}^k \mathbb{E} (U_{(j:N)})^{2/d} = \frac{1}{(N+2)(N+1)} \left[\frac{1}{3} k(k+1)(k+1) \right],$$

while for $d = 2$, it holds that

$$\sum_{j=1}^k \mathbb{E} (U_{(j:N)})^{2/d} = \frac{1}{(N+1)} \left[\frac{1}{2} k(k+1) \right].$$

In general,

$$\sum_{j=1}^k \mathbb{E} (U_{(j:N)})^{2/d} \approx (N+1)^{-2/d} \sum_{j=1}^k j^{2/d} \left(1 + \frac{2-d}{d^2 j} + \mathcal{O}\left(\frac{1}{d^2}\right) \right),$$

so that the leading order is

$$(N+1)^{-2/d} \frac{d}{d+2} k^{\frac{d+2}{d}}.$$

Equation (17) then becomes,

$$\frac{\varepsilon N^{2/d-1}}{\kappa_d} \approx \left(1 - \frac{d}{d+2} \right) k^{\frac{d+2}{d}} = \left(\frac{2}{d+2} \right) k^{\frac{d+2}{d}}$$

so that

$$\tilde{u} \approx \frac{1}{2} \left(\frac{2+d}{2\kappa_d} \right)^{\frac{2}{d+2}} \varepsilon^{\frac{2}{d+2}} N^{\frac{(2-d)^2}{d(d+2)}}$$

and then

$$u \approx \kappa_d^{\frac{d}{d+2}} \left(\frac{d+2}{2} \right)^{\frac{2}{d+2}} \varepsilon^{\frac{2}{d+2}} N^{\frac{(2-d)^2}{d(d+2)} - 2/d} = \left(\frac{\text{vol}(\mathcal{M})d}{|S^{d-1}|} \frac{(d+2)}{2} \right)^{\frac{2}{d+2}} \varepsilon^{\frac{2}{d+2}} N^{\frac{-4}{d+2}}$$

Finally, using this first order to approximately solve the equation yields the claim. \square

Proof of Theorem 1. As g is twice differentiable, we can write

$$g(X_j) = g(x_0) + L_0(x_0 - X_j) + \frac{1}{2}(X_j - x_0)^\top Q_0(X_j - x_0) + o(\|x_0 - X_j\|^2),$$

where L_0 is the gradient of g at x_0 and Q_0 is the Hessian of g evaluated at x_0 . Plugging this result in the definition of $(\Delta^{OT}g)(x_0)$, we derive

$$\begin{aligned} & (\Delta^{OT}g)(x_0) \\ &= \sum_{j=1}^N \bar{W}_{0,j}^{(f)} \left(-L_0(X_0 - X_j) - \frac{1}{2}(X_j - X_0)^\top Q_0(X_j - X_0) + o(\|X_0 - X_j\|^2) \right). \end{aligned}$$

We will split this sum into three terms and control each one separately. We will first consider the expectation and then the variance. We rewrite $W_{0,j}^\varepsilon := \bar{W}_{0,j}^{(f)}$ to streamline the notation in the proof.

Step 1: Expectation.

Let us start with the second term

$$-\frac{1}{2} \sum_{j=0}^N W_{0,j}^\varepsilon (X_j - X_0)^\top Q_0(X_j - X_0) =: B$$

The quantity in the above display is a scalar so that it is equal to its trace. Further, using the linearity and the cyclical property of the trace, it holds that

$$\begin{aligned} B &= -\frac{1}{2} \text{tr} \left[Q_0 \sum_{j=0}^N W_{0,j}^\varepsilon (X_j - X_0)(X_j - X_0)^\top \right] \\ &= -\frac{1}{2} (N+1) \text{tr} \left[Q_0 \sum_{j=0}^N \frac{(K_{\varepsilon,N} - c_{0,j})_+}{\varepsilon} (X_j - X_0)(X_j - X_0)^\top \right]. \end{aligned}$$

Using Lemma 6, it holds that

$$\begin{aligned} \mathbb{E} \sum_{j=1}^N \frac{(K_{\varepsilon,N} - c_{0,j})_+}{\varepsilon} (X_j - X_0)(X_j - X_0)^\top \\ = \frac{N}{\varepsilon} \frac{|S^{d-1}|}{d(d+2) \text{vol}(\mathcal{M})} K_{\varepsilon,N}^{\frac{d+2}{2}} K_{\varepsilon,N} \left(\begin{pmatrix} I_{d \times d} & 0 \\ 0 & 0 \end{pmatrix} + \mathcal{O}(K_{\varepsilon,N}) \right). \end{aligned}$$

Let us now address the first term, i.e.,

$$-L_0 \sum_{j=0}^N W_{i,j}^\varepsilon (X_0 - X_j).$$

The second part of Lemma B.5 in Wu and Wu (2018) reads, in our case,

$$\begin{aligned} \mathbb{E} [(X - \iota(x_0))f(X; r) \mathbf{1}\{\|X - \iota(x_0)\| \leq r\}] \\ = \frac{|S^{d-1}|}{(d+2) \text{vol}(\mathcal{M})} \left\| \left[\frac{J_{p,d}^\top \nabla f(x_0; r)}{d}, \frac{f(x_0; r) \tilde{J}_{p,p-d}^\top \mathfrak{N}(x_0)}{2} \right] \right\| r^{d+2} + \mathcal{O}(r^{d+4}). \end{aligned}$$

It follows that

$$\begin{aligned} \mathbb{E} \sum_{j=1}^N W_{0,j}^\varepsilon (X_0 - X_j) \\ = \frac{N(N+1)}{\varepsilon} \frac{|S^{d-1}|}{(d+2) \text{vol}(\mathcal{M})} \left\| \left[0, \frac{K_{\varepsilon,N} \tilde{J}_{p,p-d}^\top \mathfrak{N}(x_0)}{2} \right] \right\| K_{\varepsilon,N}^{\frac{d+2}{2}} \\ + \mathcal{O} \left(\frac{N(N+1)}{\varepsilon} K_{\varepsilon,N}^{(d+4)/2} \right). \end{aligned}$$

In view of the developments above, the expectation of the Taylor residual is negligible.

Step 2: Variance.

Let us deal with

$$-L_0 \sum_{j=1}^N W_{0,j}^\varepsilon (x_0 - X_j).$$

We have that

$$\text{Var} \sum_{j=1}^N W_{0,j}^\varepsilon (x_0 - X_j) = \frac{N(N+1)^2}{\varepsilon^2} \text{Var}((K_{\varepsilon,N} - c_{0,j})_+ (X - x_0))$$

Further,

$$\begin{aligned} \text{Var}[(K_{\varepsilon,N} - c(X, x_0))_+ (X - x_0)] \\ = \mathbb{E}[(K_{\varepsilon,N} - c(X, x_0))_+^2 (X - x_0)(X - x_0)^\top] \\ - \mathbb{E}[(K_{\varepsilon,N} - c(X, x_0))_+ (X - x_0)] \mathbb{E}[(K_{\varepsilon,N} - c(X, x_0))_+ (X - x_0)^\top] \\ = \frac{|S^{d-1}|}{d(d+2) \text{vol}(\mathcal{M})} \kappa_d^{\frac{d+2}{2}} K_{\varepsilon,N}^2 \varepsilon N^{-2} \left(\begin{pmatrix} I_{d \times d} & 0 \\ 0 & 0 \end{pmatrix} + \mathcal{O}(K_{\varepsilon,N}) \right) \\ - \frac{|S^{d-1}|^2}{(d+2)^2 \text{vol}^2(\mathcal{M})} K_{\varepsilon,N}^2 v v^\top \kappa_d^{d+2} \varepsilon^2 N^{-4} + \mathcal{O} \left(K_{\varepsilon,N}^{(d+4)/2} \varepsilon N^{-2} K_{\varepsilon,N} \right), \end{aligned}$$

where v are vectors that depend on the curvature as above. Because of the rescaling by $K_{\varepsilon,N}^{-1}$, we finally get

$$\text{Var} \left[K_{\varepsilon,N}^{-1} \sum_{j=1}^N W_{i,j}^\varepsilon (x_i - X_j) \right] = \mathcal{O} \left(K_{\varepsilon,N}^{-2} N^2 \frac{N}{\varepsilon^2} K_{\varepsilon,N}^2 N^{-2} \varepsilon \right) = \mathcal{O} \left(\frac{N}{\varepsilon} \right).$$

Let us now turn to the covariance matrix of

$$V := \text{vec} \left(\sum_j W_{i,j}^\varepsilon (x_i - X_j)(x_i - X_j)^\top \right)$$

which, using Equations (1.3.14), (1.3.16) and (1.3.31) in Kollo and von Rosen (2005), is equal to

$$N\mathbb{E}[(W_j^\varepsilon)^2(x_i - X_j) \otimes (x_i - X_j)^\top \otimes (x_i - X_j) \otimes (x_i - X_j)^\top] - NEV\mathbb{E}^\top V.$$

Relying on Lemma 7, we get that the leading order of the variance of $K_{\varepsilon,N}^{-1}V$ is

$$\mathcal{O}\left(K_{\varepsilon,N}^{-2}N^2\frac{N}{\varepsilon^2}K_{\varepsilon,N}^2K_{\varepsilon,N}^{\frac{d+4}{2}}\right) = \mathcal{O}\left(\frac{NK_{\varepsilon,N}}{\varepsilon}\right).$$

The claim follows. \square

B Numerical experiments

B.1 Simulations for optimal dual potentials

We exhibit the behaviour of the optimal potentials for N random points on the d -sphere and various values of the parameter ε . In $d = 1, 2, 3$, $N = 10^3$ points were sampled uniformly from S^d by sampling first a standard Gaussian in \mathbb{R}^{d+1} and scaling to unit norm. We numerically solved the corresponding discrete optimal transport problem with ε in the range $[10^{-2}, 10^6]$ and plotted $\log(\bar{u})$ against $\log(\varepsilon)$, where \bar{u} denotes the averaged value of the resulting dual potential over the N points. For ε sufficiently large, we estimated the exponent α for the relationship $u \sim \varepsilon^\alpha$. Our empirical findings agree with the exponent $\frac{2}{2+d}$.

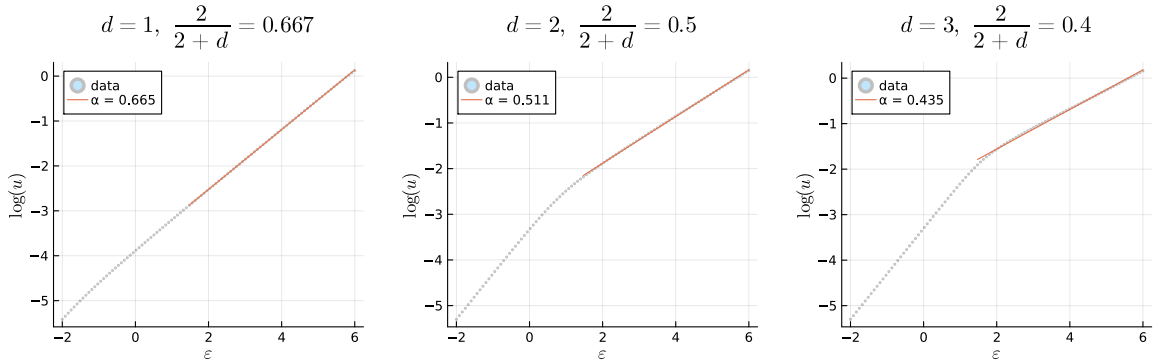


Figure 4: Scaling of dual potential u on the d -sphere, for $d = 1, 2, 3$.

B.2 Behaviour of the operator

Next, we investigate the behaviour of the operator Δ^{OT} in the discrete setting where points are sampled from the uniform distribution on the 2-dimensional torus with major and minor radii $R = 1, r = 1/2$. We fix a point $(0, 1, 1/2)$ at which the tangent space $T_{x_0}\mathcal{M}$ is spanned by (e_1, e_2) . We then consider a function $f(x, y, z) = \frac{1}{2}(3x^2 + 5y^2 + 7z^2)$. For $N = 100, 250, 500, 1000, 2500, 5000, 10,000$ points sampled uniformly from the torus, we calculated the $(N + 1) \times (N + 1)$ coupling π by solving (7) and then computed the quantity $K_{\varepsilon,N}^{-1}(\Delta^{OT}f)(x_0)$.

Motivated by the asymptotic scalings we derived, we tried setting $\varepsilon \propto N^\alpha$ for varying exponents: $\alpha = 2$ which should correspond to a fixed regularisation level in the continuous case (and we do not expect convergence to the Laplacian in this case), and $\alpha = 1.75, 1.5, 1.25$ which all fall within the regime where the results of Section 1 apply. We show in Figure 5 the values of $K_{\varepsilon,N}^{-1}(\Delta^{OT}f)(x_0)$ over 25 independent samples at each value of N .

We see that when $\alpha = 2$, the quantity $K_{\varepsilon,N}^{-1}(\Delta^{OT}f)(x_0)$ stabilises around a fixed value close to zero as N increases. This agrees with our understanding that $\varepsilon \propto N^2$ in the discrete setting corresponds to the continuous case of empirical distributions with a fixed value of ε . On the other hand, when $1 < \alpha < 2$ we observe a pattern of values appears to converge around a different, positive, value. Importantly, for various $1 < \alpha < 2$, these values are similar – this supports the scaling relation of Theorem 1 and suggests that the quantity is converging to the value (up to a constant independent of ε, N) of the Laplace–Beltrami operator at x_0 . As a local averaging process takes place, setting ε too small means implies smaller neighbourhoods and thus a larger variances as is exhibited on the bottom right panel of Figure 5.

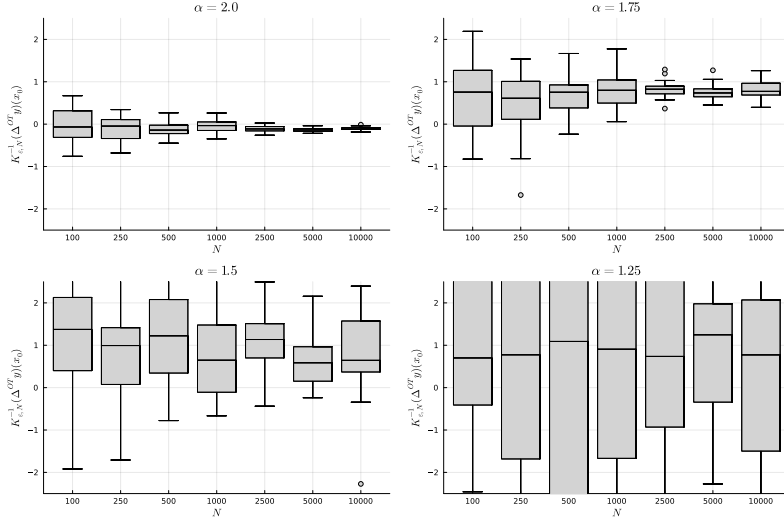


Figure 5: Estimate of Laplacian $K_{\epsilon, N}^{-1}(\Delta^{OT} f)(x_0)$ for varying sample sizes N , and $\epsilon \propto N^\alpha$, for various choices $\alpha = 2, 1.75, 1.5, 1.25$.

C Computational scheme

To solve the dual problem (6), the algorithm proposed by Lorenz, Manns, and Meyer (2021, Algorithm 2) can be adapted to the symmetric case in which case a single dual potential is solved for. We detail this below in Algorithm 1, and notably the symmetry halves the size of the linear system (19). Since we seek a projection onto the set of *hollow* bistochastic matrices and not the set of bistochastic ones, the dual problem involves a term $\mathbf{1}\mathbf{1}^\top - I$.

For large datasets, we show that this method is amenable to an active set method like the one proposed in (Lim, Vidal, and Haeffele, 2020). This allows us to take advantage of the sparse nature of the bistochastic projection in Frobenius norm: most computations are done explicitly in terms of sparse matrices. We introduce a sparse support matrix $S \in \{0, 1\}^{N \times N}$ and write $S^c = 1 - S$. Consider then the primal problem with support restricted to S :

$$\min_{A \in \mathcal{K}, A \odot S^c = 0} \|A + \epsilon^{-1}C\|_F^2. \quad (20)$$

If the feasible set for the restricted-support primal problem (20) has nonempty relative interior, the corresponding dual problem exists and strong duality holds, e.g. by Slater's condition. The corresponding dual problem is written:

$$\max_u \langle u, \mathbf{1} \rangle - \frac{1}{4\epsilon} \|[u\mathbf{1}^\top + \mathbf{1}u^\top - C]_+ \odot S\|_F^2. \quad (21)$$

In the above, we have absorbed the hollow constraint on the diagonal into the support matrix S by assuming that $S_{ii} = 0$ for all i . The problem (21) can be tackled using the same semi-smooth Newton algorithm as proposed in Algorithm 1. The restriction on the support of A can be formally understood as setting $C_{ij} = +\infty$ whenever $S_{ij} = 0$. The benefit of this approach is that solution of each restricted-support problem by the semismooth Newton algorithm 1 involves only $\mathcal{O}(|S|)$ nonzero entries, rather than $\mathcal{O}(N^2)$ in the dense case. For N larger than a few thousand, we find that this leads to significant speedups. As proved by the analysis in (Lim, Vidal, and Haeffele, 2020, Lemma 1, Proposition 2), it is sufficient to use bistochasticity of the primal solution as a stopping condition for 2 and convergence within a finite number of steps is guaranteed. The critical factor for good behaviour in 2 is the choice of initial support set S , in particular for duality to hold the support set $\{A : A \in \mathcal{K}, A \odot S^c\}$ must remain feasible. This is discussed at length in Lim, Vidal, and Haeffele, 2020, Section A.3; in practice we find good results by initialising S with k -nearest neighbours as an initial rough guess, and adding random permutation matrices to ensure feasibility.

As a basic demonstration of the computational speedup achieved by implementation of Algorithm 2, we sample $N = 25,000$ points from a standard Gaussian distribution in dimension $d = 100$ and form the matrix C of pairwise squared Euclidean distances. We normalise C to have mean 1, and use Algorithms

Algorithm 1 Algorithm 2 of Lorenz, Manns, and Meyer, 2021, specialised to symmetric inputs

Input: cost matrix $C_{ij} \geq 0$, regularisation parameter $\varepsilon > 0$, Armijo parameters $\theta, \kappa \in (0, 1)$, conjugate gradient regulariser $\delta = 10^{-5}$.

Initialise: $u \leftarrow \mathbf{1}$

$$\Phi(u) = -\langle u, \mathbf{1} \rangle + \frac{1}{4\varepsilon} \| [u\mathbf{1}^\top + \mathbf{1}u^\top - C]_+ \|_2^2. \quad (18)$$

while not converged **do**

$$P_{ij} \leftarrow u_i + u_j - C_{ij}$$

$$\sigma_{ij} = \mathbf{1}\{P_{ij} \geq 0\}$$

$$\pi_{ij} = \max\{P_{ij}, 0\}/\varepsilon$$

Solve for Δu :

$$(\sigma + \text{diag } \sigma \mathbf{1} + \delta I) \Delta u = -\varepsilon(\pi - I)\mathbf{1}. \quad (19)$$

Set $t = 1$ and compute

$$d = \varepsilon \sum_{ij} \pi_{ij} [(\Delta u)_i + (\Delta u)_j] - 2\varepsilon \langle \Delta u, \mu \rangle$$

while $\Phi(u + t\Delta u) \geq \Phi(u) + t\theta d$ **do**

$$t \leftarrow \kappa t$$

end while

$$u \leftarrow u + t\Delta u$$

end while

$$\pi_{ij} = \max\{0, u_i + u_j - C_{ij}\}/\varepsilon$$

1 and 2 to compute the bistochastic Frobenius projection with parameter $\varepsilon = 1$. For Algorithm 2, we initialise the support using k -nearest neighbours with $k = 50$. On an Intel Xeon Gold 6242 CPU @ 2.80GHz with 16 cores and 64 GB memory, we find the computation time to be 743 seconds (Algorithm 1) and 86 seconds (Algorithm 2, including the time taken to initialise the support) respectively. Doubling the number of points to $N = 50,000$, Algorithm 1 runs out of memory while Algorithm 2 runs successfully in 313 seconds. Further speedups could be achieved by optimisation of numerical routines for better memory efficiency or using GPU hardware (Lim, Vidal, and Haeffele, 2020).

Algorithm 2 Active-set method based on Lim, Vidal, and Haeffele, 2020, Algorithm 2

Input: initial support set $S_{ij} \in \{0, 1\}$, cost matrix $C_{ij} \geq 0$, regularisation parameter $\varepsilon > 0$, Armijo parameters $\theta, \kappa \in (0, 1)$, conjugate gradient regulariser $\delta = 10^{-5}$.

$$u^0 \leftarrow \mathbf{1}$$

$$S^0 \leftarrow S$$

$$k \leftarrow 1$$

while π^k is not bistochastic **do**

Solve for dual potential u^k (21) using Algorithm 1, started from u^{k-1} and support set S^{k-1} .

$$\pi_{ij}^k \leftarrow \max\{0, u_i^k + u_j^k - C_{ij}\}/\varepsilon$$

$$S^k \leftarrow S^{k-1} \cup \text{supp}(\pi^k)$$

$$k \leftarrow k + 1$$

end while

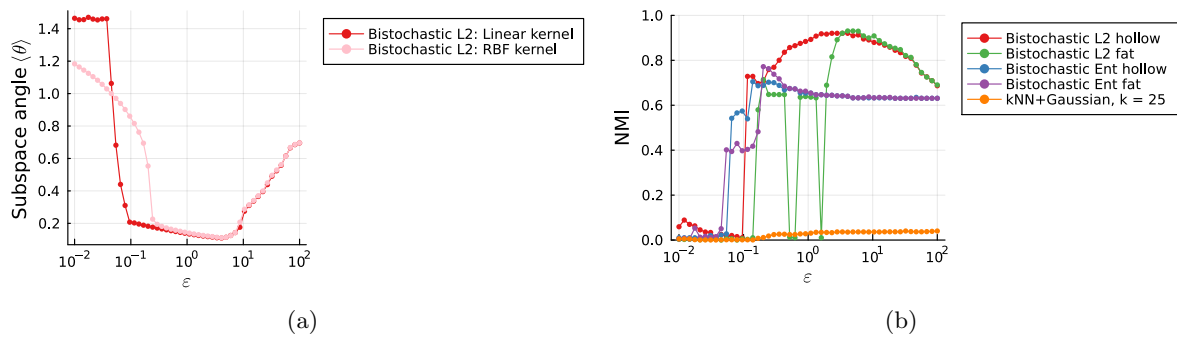


Figure 6: (a) For spiral example: comparison of linear kernel $K(x, y) = \langle x, y \rangle$ to Gaussian RBF kernel $K(x, y) = \exp(-\|x - y\|_2^2)$ with Frobenius projection. (b) For Gaussian mixture model example: comparison of clustering performance of hollow bistoochastic projection to *fat* bistoochastic projection.